

# Development of a Novel Magnetic Clutch Thruster

by

© Jonathan Smith

A thesis submitted to the School of Graduate Studies  
in partial fulfillment of the requirements  
for the degree of Master of Engineering

Faculty of Engineering and Applied Science

Memorial University of Newfoundland

April 2024

St. John's, Newfoundland

© Copyright by Jonathan Smith, 2022  
All Rights Reserved.

## ACKNOWLEDGMENTS

First, I would like to express my deepest gratitude to my supervisor, Dr. Michael Hinchey, for his patience, invaluable academic guidance, enthusiastic encouragement, and help throughout my studies at MUN. With his insight, support, and suggestions, I have developed a good knowledge and interest in my research field. I am also grateful that I have had the opportunity to work on many of his projects, and I hope to continue participating in his future work.

I want to thank Dr. Doug Smith for taking me on as a student and allowing me the guidance I needed to finish this and finally start a new chapter of my life. I would also like to thank the late Paul Morrissey for supporting my work. His work term was my first real Engineering undertaking, and he is greatly missed.

My gratitude is also extended to Dave Snook, Tom Pike, Trevor Clark, Matt Curtis, and Craig Mitchell for their kind help during the stages of this project. In addition, I want to thank graduate student Ashim Ali for his help with OpenFoam CFD.

I want to thank my wife, Gracie, for her support and concern for my academic research and life. Moreover, I would like to thank my parents for their unconditional love, support, and understanding during my studies.

## ABSTRACT

This thesis describes the comprehensive process of designing, constructing, and testing a fully enclosed magnetic clutch thruster concept model for an autonomous underwater vehicle. Originally conceived as an enhancement to a pre-existing unit developed by Dr. Hinchey, the project faced various limitations in terms of equipment selection and physical sizing. The primary objective was to demonstrate the feasibility of such a design within these constraints.

The design phase involved modeling in SolidWorks, followed by fabrication using a combination of 3D printing and machining services aided by Technical Services at MUN. Additionally, testing unit structures were engineered and tailored specifically for this project. Evaluation procedures were carried out in the Engineering Fluids Lab at MUN using self-designed and constructed equipment.

Upon completion, the thruster underwent a series of rigorous tests aimed at collecting and analyzing data for comparison. These extensive model tests, conducted with the thruster integrated into our testing structure and measured with a load cell, revealed maximum responses and excellent repeatability. Further verification testing was undertaken to ensure the credibility of our testing apparatus and setup.

The collected data was subsequently compared against model-based computational fluid dynamics (CFD) simulations, validating our concept and solid evidence of the results obtained through real-world testing. This thesis comprehensively explores the design, construction, and testing processes involved in developing an innovative thruster concept for autonomous underwater vehicles.

## TABLE OF CONTENTS

ACKNOWLEDGMENTS .....	iii
ABSTRACT.....	iv
LIST OF TABLES.....	vii
LIST OF GRAPHS .....	viii
LIST OF EQUATIONS .....	ix
LIST OF ABBREVIATIONS.....	xiii
CHAPTER 1: Introduction .....	14
History of Project .....	14
Current Work.....	16
Project Constraints .....	17
Thesis Structure Outline.....	18
CHAPTER 2: Literature Review .....	21
Introduction .....	21
Introduction to AUVs and Thruster Technology .....	22
Challenges and Limitations of Mechanically Sealed Thrusters in AUVs.....	22
Magnetic Clutches.....	24
Magnetic Forces .....	27
CHAPTER 3: Design and Fabrication of a Prototype .....	30
CHAPTER 4: Testing of The Thruster .....	41
Fabrication of Test Frames.....	41
Description of the Bench Test.....	42
Horizontal Support Structure .....	43
Vertical Beam with Pivot Connection.....	43
Electronics.....	45
Load Frames.....	46
Test Results .....	49
Difference Caused by Submerged Level.....	50
Difference of Forward and Reverse .....	51
Duct Efficiency .....	51

Torque Output .....	52
Wall Interference .....	53
Proof Of Concept .....	54
CHAPTER 5: CFD Validation.....	56
Overview of CFD .....	56
Governing Equations.....	56
OpenFOAM CFD .....	59
CFD Results .....	60
CHAPTER 6: Conclusions and Future Work .....	63
Conclusions .....	63
Future Work .....	64
REFERENCES .....	66
APPENDICES .....	68
Appendix A: Test Calibrations.....	68
Appendix B: Raw Test Data .....	77
Appendix C: Openfoam Menus.....	86
Appendix D: Hydrodynamic Bearing .....	92
Appendix E: Simple Propeller Model .....	95
Appendix F: Hull Hoop Stress .....	98

## LIST OF TABLES

Table 4.1 <i>Tank Depth and Wall Distance</i> .....	49
Table A.1 <i>RPM Measurements</i> .....	69
Table A.2 <i>Slip and Torque Test Results</i> .....	71
Table A.3 <i>Horizontal Results</i> .....	73
Table A.4 <i>Vertical Results</i> .....	73

## LIST OF GRAPHS

Graph 4.1 <i>Thrust for Different Submergence Levels</i> .....	50
Graph 4.2 <i>Comparison of Forward versus Reverse</i> .....	51
Graph 4.3 <i>Influence of the Shroud</i> .....	52
Graph 4.4 <i>Torque Load</i> .....	53
Graph 4.5 <i>Wall Interference</i> .....	54
Graph 5.1 <i>Thrust and Torque Results</i> .....	61
Graph A.1 <i>Magnet Load vs Angle</i> .....	75
Graph B.1 <i>Test 1 Results</i> .....	77
Graph B.2 <i>Test 2 Results</i> .....	78
Graph B.3 <i>Test 3 Results</i> .....	79
Graph B.4 <i>Test 4 Results</i> .....	80
Graph B.5 <i>Test 5 Results</i> .....	81
Graph B.6 <i>Test 6 Results</i> .....	82
Graph B.7 <i>Test 7 Results</i> .....	83
Graph B.8 <i>Test 8 Results</i> .....	84
Graph B.9 <i>Test 9 Results</i> .....	85



## LIST OF EQUATIONS

Equation 2.1 <i>Force between Two Point Magnets</i> .....	28
Equation 2.2: <i>Combined Strength Force</i> .....	28
Equation 2.3 <i>Distance between Magnets</i> .....	28
Equation 2.4 <i>Radial and Tangential Force Components</i> .....	29
Equation 2.5 <i>Force of Two Identical Bar Magnets</i> .....	29
Equation 4.1 <i>Percent Error</i> .....	
Equation 5.1 <i>Conservation of Mass</i> .....	57
Equation 5.2 <i>Conservation of Momentum</i> .....	57
Equation 5.3 <i>The <math>k\epsilon</math> Turbulence Model</i> .....	57
Equation 5.4 <i>Material Volume of Fluid</i> .....	58
Equation 5.5 <i>Partial Differential Equation for CFD</i> .....	58
Equation 5.6 <i>Time Stepping Scheme</i> .....	58
Equation D.1 <i>Reynolds Equation</i> .....	93
Equation D.2 <i>Thrust Bearing Case</i> .....	93
Equation D.3 <i>Blocked Sides Case</i> .....	94
Equation D.4 <i>Step Bearing Case</i> .....	94
Equation D.5 <i>Simplified Step Case</i> .....	94
Equation D.6 <i>Step Pressure</i> .....	94
Equation E.1 <i>Jet Thrust Equation</i> .....	96
Equation E.2 <i>Flow Geometry</i> .....	96
Equation E.3 <i>Jet Speed Equation</i> .....	96

Equation F.1 <i>Hoop Stress Equation</i> .....	99
Equation F.2 <i>External Pressure</i> .....	99
Equation F.3 <i>Pressure Depth Law</i> .....	99
Equation F.4 <i>Operation Depth</i> .....	100

## LIST OF FIGURES

Figure 1.1 <i>Original AUV</i> .....	15
Figure 2.1 <i>Axial Clutch</i> .....	25
Figure 2.2 <i>Radial Clutch</i> .....	25
Figure 2.3 <i>Generic Magnetic Clutch Thruster</i> .....	26
Figure 2.4 <i>Generalization of Magnetic Clutch</i> .....	27
Figure 3.1 <i>Magnetic Clutch Arrangement</i> .....	30
Figure 3.2 <i>Magnetic Clutch Arrangement CAD</i> .....	31
Figure 3.3 <i>Magnetic Clutch Arrangement</i> .....	31
Figure 3.4 <i>Neodymium Magnets</i> .....	32
Figure 3.5 <i>Geared DC Brush Motor</i> .....	33
Figure 3.6 <i>DC Motor Holder</i> .....	33
Figure 3.7 <i>Stainless Steel Pipe</i> .....	34
Figure 3.8 <i>Delrin End Caps with O rings</i> .....	35
Figure 3.9 <i>Waterproof Subcon Connection</i> .....	36
Figure 3.10 <i>3D Printed Propeller</i> .....	36
Figure 3.11 <i>3D Printed Shroud</i> .....	38
Figure 3.12 <i>Hydrodynamic Bearing</i> .....	39
Figure 3.13 <i>General Spacer CAD Model</i> .....	39
Figure 3.14 <i>Final Thruster Schematic</i> .....	40
Figure 3.15 <i>Fabricated Prototype</i> .....	40
Figure 4.1 <i>Bench Test Set Up</i> .....	41
Figure 4.2 <i>Fluid Lab Deep Tank Set Up</i> .....	44

Figure 4.3 <i>Knife Edge Fulcrum</i> .....	45
Figure 4.4 <i>Electronic Scale</i> .....	45
Figure 4.5 <i>Power Supply</i> .....	46
Figure 4.6 <i>Thrust Frame</i> .....	47
Figure 4.7 <i>Torque Frame</i> .....	48
Figure 5.1 <i>ParaFoam Results</i> .....	61
Figure A.1 <i>Tachometer</i> .....	68
Figure A.2 <i>Reflective Tape Set up</i> .....	69
Figure A.3 <i>Slip and Torque Test Set up</i> .....	70
Figure A.4 <i>Balance Test Set Up</i> .....	72
Figure A.5 <i>Magnet Point Load Test Set Up</i> .....	74
Figure A.6 <i>CFD Streamline</i> .....	76
Figure A.7 <i>Red Dye Test</i> .....	77
Figure C.1 <i>Run Window</i> .....	86
Figure C.2 <i>Eddy Folder Contents</i> .....	87
Figure C.3 <i>0.orig Folder Contents</i> .....	87
Figure C.4 <i>Constant Folder Contents</i> .....	88
Figure C.5 <i>TriSurface Subfolder Contents</i> .....	89
Figure C.6 <i>Dynamic Meshes</i> .....	90
Figure C.7 <i>System Folder Contents</i> .....	90
Figure E.1 <i>Velocity Vector Diagram</i> .....	96

## LIST OF ABBREVIATIONS

AUV .....	Autonomous Underwater Vehicle
CAD .....	Computer-Aided Design
DC .....	Direct Current
CFD.....	Computational Fluid Dynamics
MUN .....	Memorial University of Newfoundland
MPA .....	Megapascal
NdFeB.....	Neodymium
DSCL .....	Dynamical System and Control Laboratory
OpenFoam.....	Opensource Field Operation
GUI .....	Graphical User Interface
MATLAB.....	Matrix Laboratory
3D.....	Three-Dimensional
VOF.....	Volume of Fluid
PDE.....	Partial Differential Equation

# CHAPTER 1

## INTRODUCTION

### History of Project

In 2008, Jonathan Smith joined Dr. Michael Hinchey's team as a work term student to undertake the design and fabrication of a small waterproof propeller for an autonomous underwater vehicle (AUV). This propeller, which was an integral part of the project, was intended to help balance the vehicle in the water by using a buoyancy pump and two DC motors for horizontal movement control. While conventional open DC motors suffice for freshwater applications, the project's scope mandated the AUV's adaptation for saltwater environments, posing challenges related to corrosion and conductivity. To address these concerns, it became imperative to encase the motors to prevent liquid ingress. Eschewing shaft seals due to wear and maintenance considerations, a waterproof solution was sought using magnetic couplings that utilize magnetic forces for torque transmission without the need for a mechanical connection.

During the course of the project, the development of magnetic couplers primarily relying on magnetic attraction began to enter the market. However, before this project began, there was no established method that utilized the force of attraction. In the search for a streamlined and simplified approach for stabilizing the output shaft, the decision was made to opt for repulsion force-based couplers, a novel concept in the field. A detailed exploration of this approach is documented in the Literature Review section.



*Figure 1.1 Original AUV*

After narrowing down the scope of the project to a specific component of the AUV, namely the design, fabrication, and testing of the magnetic clutch thruster, the author embarked on a comprehensive endeavor. The primary objective was to develop a concept model that would validate the feasibility of the closed magnet clutch system. This involved meticulous consideration of factors such as efficiency and optimization of components,

including duct and propeller design. The project maintained a singular focus on demonstrating the functionality and feasibility of the device as a concept without engaging in comparative analyses with commercially available models.

Commencing this project as a full-time master's student in 2010 the author's dedication remained unwavering despite subsequent transitions. Upon completing the required courses, employment opportunities with an offshore oil company led to a change to part-time student status. A personal commitment necessitated a temporary leave of absence between 2015 and 2021, but the project remained a priority. In 2021, resuming full-time status in response to industry dynamics and a decline in the oil industry, the author ensured the project's timely completion despite the extended timeline. This adaptive approach to academic and professional commitments underlines the author's commitment to the academic work and completion of the project.

### **Current Work**

The main objective of this MEng project was to develop and appraise a conceptual model for the assembly of the propeller, its viability based on a preliminary appraisal, and to assess critical design changes arising from established precedents that indicate necessary improvements to the model. These differences are to be validated through Computational Fluid Dynamics (CFD), aimed at obtaining additional valuable information required with a comprehensive theoretical basis and practical relevance for the goals of the project. The project also aimed to develop a propeller design that would be in a position to hold an even pitch during reverse operations as it does in forward operations, hence even blade angles at all conditions.



#### **Four main areas of development for this project were:**

- Design of the Concept Model: This involved creating the initial CAD work and conceptual framework for the project.
- Fabrication of the Concept Model: This phase encompassed selecting materials, manufacturing components, and assembling the model according to the design specifications.
- Testing of the Concept Model: Rigorous testing was conducted to evaluate its functionality. Testing protocols were designed to simulate real-world conditions.
- Validation using CFD (Computational Fluid Dynamics): In addition to physical testing, computational analysis using CFD was employed to further validate the concept model's design. CFD simulations provided insights into fluid flow behavior, and other relevant factors. This data could be used to help refine and optimize the model for enhanced performance.

#### **Project Constraints**

Key constraints significantly impacting this project included:

**Size:** The original design specifications for the Autonomous Underwater Vehicle (AUV) dictated portability and ease of handling by a single individual. Consequently, all developments were constrained to smaller scales to avoid bulkiness. Moreover, as all tests were slated for the lab's deep tank, precautions were taken to ensure tank conditions did not compromise test results.

**Materials:** Initial project funding from Land & Sea Enterprises via an Industrial Outreach Grant at MUN provided resources such as magnets, motors, and parts fabrication.

Subsequent project phases necessitated the utilization of available materials and equipment to maintain cost-effectiveness.

**Machinability:** Construction and machining were predominantly conducted in-house to optimize expenses, leveraging Memorial's various laboratories. Complex components, such as bearings, were selectively outsourced and machined by Memorial's technical services.

**Software:** Changes in software accessibility, particularly the unavailability of previously used software like Flow3d from Flow Sciences, prompted the adoption of open-source software for Computational Fluid Dynamics (CFD) analyses, requiring adaptation and learning.

**COVID-19:** The global pandemic introduced significant challenges to the study, including disruptions in shipping schedules, limited availability of faculty, and restricted access to university services, impeding project progress.

## **Thesis Structure Outline**

### **Chapter 1: Introduction**

This chapter serves as an introduction to the work and offers the reader an insight into the historical backdrop of the project. It delves into the origins of the research endeavor and delineates the overarching objectives pursued. In addition, the scope of the work is precisely defined and delineated in this chapter, providing clarity on the boundaries and focus areas of the study.

## **Chapter 2: Literature Review**

A comprehensive exploration of the pertinent background material forms the cornerstone of this chapter. Drawing on existing scholarly works, this section provides the reader with a nuanced understanding of the theoretical underpinnings of the project. Through an extensive review of the literature, the main concepts, theories, and methods relevant to the research are explained and contextualized.

## **Chapter 3: Design And Fabrication Of A Prototype**

In this chapter, meticulous attention is devoted to detailing the design processes and methodologies employed in conceiving the conceptual model. From conceptualization to design refinement, this chapter provides an in-depth exploration of the fabrication phase of the concept model. By examining the fabrication techniques, material selection and manufacturing processes, readers will gain a comprehensive understanding of the intricate steps involved in bringing the conceptual design to fruition.

## **Chapter 4: Testing Of The Thruster**

This chapter provides an in-depth exploration of the fabrication phase of the concept model. A meticulous examination of fabrication techniques, materials selection, and manufacturing processes gives readers a comprehensive understanding of the intricate steps involved in bringing the conceptual design to fruition.

## **Chapter 5: Testing**

The testing phase of the physical model takes center stage in this chapter. Beginning with a comprehensive overview of the test frames developed explicitly for this purpose, the chapter presents and analyzes the data obtained from the conducted tests. Additionally, an error

analysis of the collected data offers valuable insights into the reliability and validity of the experimental findings.

### **Chapter 5: Computational Fluid Dynamics (CFD) Validation**

This chapter presents a mathematical validation of the experimental findings through Computational Fluid Dynamics (CFD) simulations. Through detailed analyses and comparisons with empirical data, the chapter elucidates the extent to which the simulated results corroborate the experimental observations, thus bolstering the credibility of the study outcomes.

### **Chapter 6: Conclusions and Future Directions**

The final chapter summarizes the results of the study, draws overarching conclusions and reflects on the implications of the research findings. In addition, the chapter provides valuable insights into potential avenues for future research and offers recommendations and suggestions for further investigation in the field.

## **CHAPTER 2:**

### **LITERATURE REVIEW**

#### **Introduction**

For this systematic review, the literature surrounding the design of the thruster will be discussed. This literature review aimed to answer the following research questions: How will the thruster work, and how is it different from others.

The primary innovation highlighted in this study is the development of a magnetic clutch tailored for small propellers. Originating from my original conceptual design circa 2010, the design is updated, but the concept stays the same. The literature review examines the landscape of magnetic clutch technology around 2010, excluding any post-2010 advancements, as they are considered insignificant to the scope of this study. Notably, as featured in our clutch design, the lack of analytical solutions in the existing literature for bar magnets arranged at arbitrary angles to each other presented a notable challenge. However, we endeavored to adapt the simplified analysis applicable to two-point magnets for our purposes, elaborated further in this report.

Our analysis considered the use of computer-based tools like ANSYS for their potential in detailed analysis. Still, their complexity and the required learning curve did not align with the objectives of our study. Consequently, our approach favored the use of materials that were readily available in the early design stages to minimize the need for extensive material sourcing. Opting for custom-made materials was considered financially impractical, which emphasizes the importance of detailing the properties of the selected magnets in this report.

In addition, the thruster design in this study features a specialized propeller engineered to deliver consistent thrust in both forward and reverse directions. Although an in-depth discussion of propeller theory is beyond the scope of this thesis, we have incorporated blade deflector theory and Computational Fluid Dynamics (CFD) approaches in the development of the propeller. The application and implications of these methods are discussed in more detail in the CFD chapter of this report.

### **Introduction to AUVs and Thruster Technology**

Autonomous Underwater Vehicles (AUVs) are pivotal in various underwater tasks, ranging from scientific research to commercial and military applications. At the heart of the maneuverability and performance of AUVs lies their thrusters, which enable navigation and stability in underwater environments.

Traditional mechanically sealed thrusters have been a staple in AUV designs, providing the necessary propulsion through mechanical means. However, these systems face challenges such as wear and tear and the risk of leakage, which can compromise the AUV's functionality and longevity.

Magnetic variants demonstrate superior efficiency, reliability, and performance when comparing magnetic and mechanical thrusters. This technological shift can significantly improve the capabilities of AUVs and enable more complex and prolonged underwater missions.

### **Challenges and Limitations of Mechanically Sealed Thrusters in AUVs**

Mechanically sealed thrusters have been fundamental to the development and operation of Autonomous Underwater Vehicles (AUVs). However, they come with inherent

challenges and limitations that can affect the efficiency and reliability of these underwater systems.

**Wear and Tear:** One of the primary issues with mechanically sealed thrusters is the wear and tear of the moving parts. Due to continuous operation in varying and often harsh underwater environments, these mechanical components are prone to degradation. This can lead to reduced efficiency and an increased need for maintenance and replacements, as highlighted in studies on the design and operation of AUVs.

**Risk of Leakage:** By their nature, mechanical seals have a risk of leakage. This risk is exacerbated in underwater environments where pressure differentials are significant. Leaks can lead to water ingress, damaging internal components and systems, potentially leading to mission failure or loss of the AUV. The reliability of mechanical seals in long-duration missions is a critical concern.

**Hydrodynamic Limitations:** The design of mechanically sealed thrusters often encounters hydrodynamic limitations. The interaction between the moving parts and the water can create additional drag and reduce the overall efficiency of the AUV. Optimizing the hydrodynamic efficiency of these thrusters is a complex task that requires careful consideration of the design of the thruster and its interaction with the vehicle hull.

**Maintenance and Operational Costs:** Mechanically sealed thrusters require regular maintenance to ensure their functionality. This maintenance can be costly and time consuming, especially for AUVs deployed in remote or hard-to-reach areas. The operational costs associated with maintaining and repairing these thrusters can significantly impact the overall budget of AUV missions.

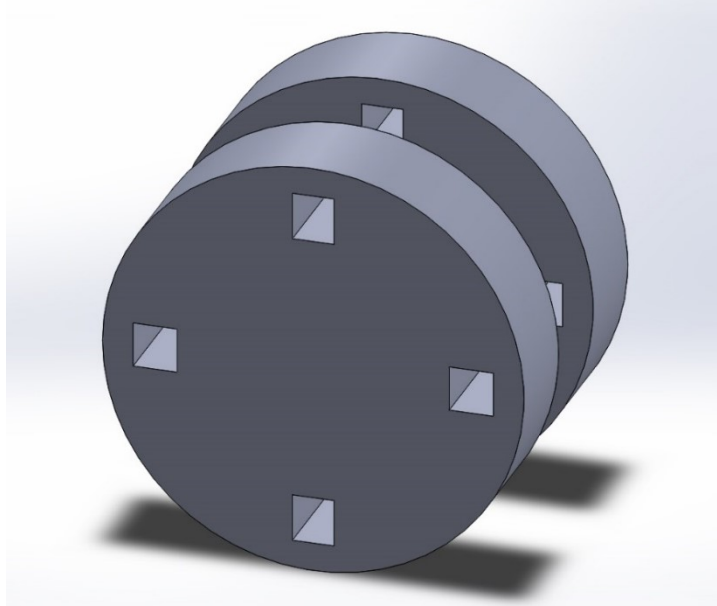
Limited Depth and Pressure Capabilities: Mechanical thrusters have limitations regarding the depths they can operate at and the pressure they can withstand. As AUVs are deployed in increasingly deep and pressurized environments, the mechanical components of these thrusters must be designed to withstand these extreme conditions, which can be challenging and costly.

While mechanically sealed thrusters have been instrumental in the development of AUVs, their limitations in terms of wear and tear, risk of leakage, hydrodynamic efficiency, maintenance costs, and depth capabilities pose significant challenges. These challenges have sparked interest in alternative thruster technologies, such as magnetic thrusters, which promise improved performance and reliability for AUV operations.

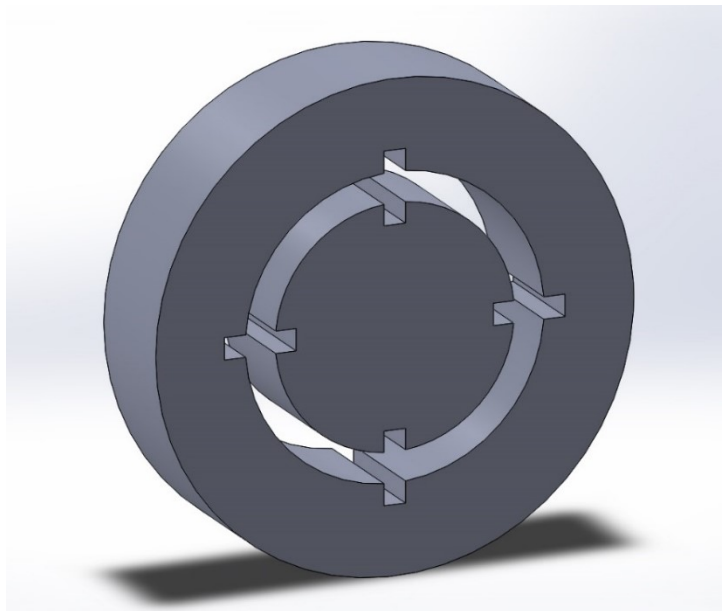
### **Magnetic Clutches**

Figure 2.1 & 2.2 illustrate two potential configurations of magnetic clutches: axial and radial. In the axial clutch arrangement, sets of magnets on the rotors are separated by an axial gap, whereas in the radial clutch configuration, the magnets are separated by a radial gap. Tecnydyne, a prominent manufacturer, is recognized for pioneering the integration of magnetic clutches into thruster systems. Notably, the smallest thruster model manufactured by Tecnydyne, depicted in Figure 2.3, employs an axial clutch and shares a comparable size with the prototype developed for this thesis. Notably, this model did not exist at the commencement of the thesis project nor during the conceptualization of its fundamental design.





*Figure 2.1 Axial Clutch*



*Figure 2.2 Radial Clutch*

In Tecnadyne's clutch mechanism, the magnetic attraction between the magnets on the inner and outer rotors facilitates engagement. Precision bearings are crucial in preventing the magnets from adhering together. Conversely, our thruster incorporates a radial clutch

design, where the repulsion forces propel the outer rotor around the inner rotor, so no separate bearings are required as the magnets take over this function.



*Figure 2.3* Generic Magnetic Clutch Thruster

A critical consideration in magnetic clutch design is to ensure that the maximum torque exceeds the normal hydrodynamic torque of the propeller. Failure to meet this requirement may result in slippage between the inner and outer rotors, impeding the propeller's desired rotational speed. To protect the motor from burning out, the maximum torque of the magnetic clutch should also remain below the full torque capacity of the motor. This precaution ensures that the motor can continue to operate even if the propeller becomes jammed or stalled during operation.

## Magnetic Forces

Figure 2.4 illustrates a generic radial magnetic clutch. This one has four magnets inside the hull and four outside. They are all aligned radially.

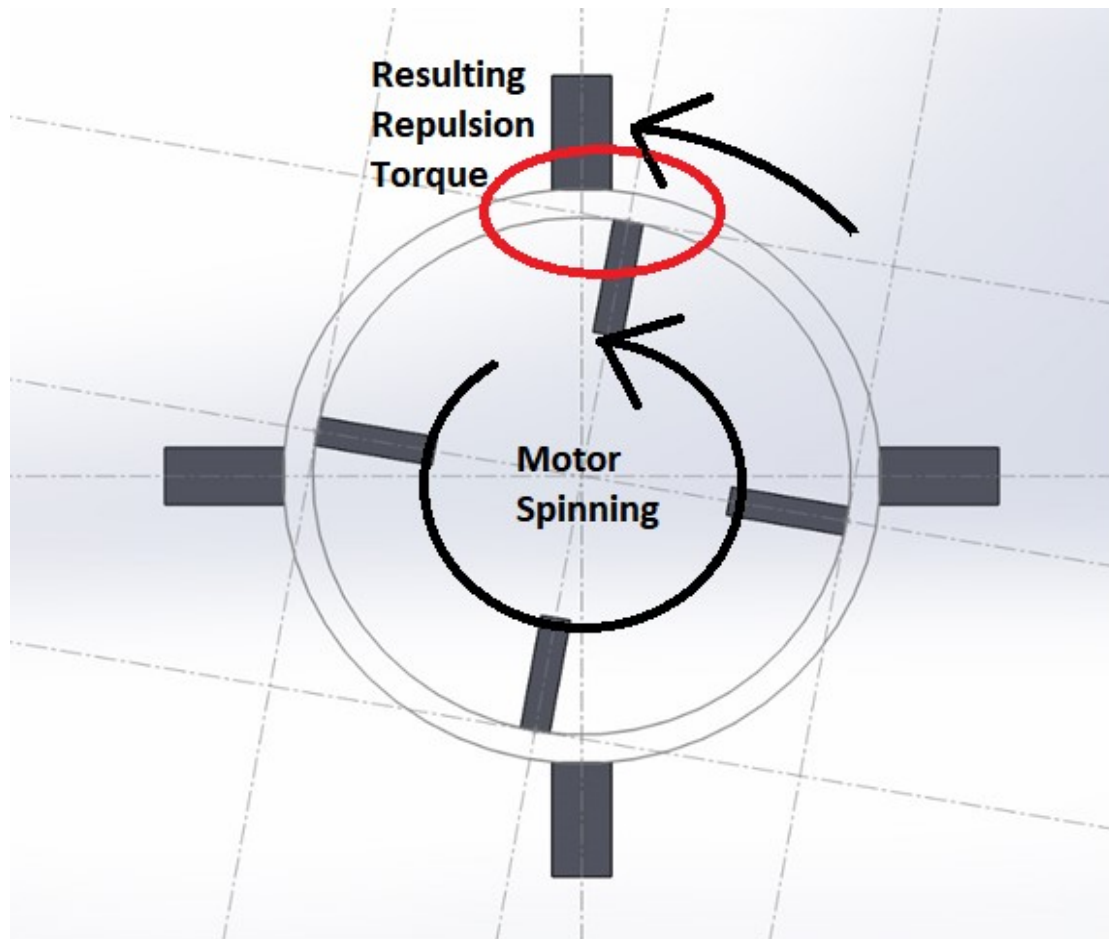


*Figure 2.4* Generalization of Magnetic Clutch

The energy calculation is typically approximated to facilitate interactions along elementary dipoles in the simulation of magnetic forces within an array of magnetic elements. Such interactions, known as Magnetostatic interactions, govern the forces between cylindrical permanent magnets (Vokoun et al., 2009). The repulsive force between two-point

magnets can be computed by considering both magnets' total magnetostatic interaction energy, or "strength," The following equation defines this relationship.

$$F = \frac{[q_1 q_2]}{d^2}$$

*Equation 2.1 Force between Two Point Magnets*

In this context,  $q_1$  and  $q_2$  represent the respective strengths of the magnets, while  $d$  denotes the radial distance between them, measured in meters (SI unit). It is reasonable to assume that the magnets are composed of the same material, exhibiting uniform magnetization along their axis and characterized by saturation magnetization. In scenarios where the strengths remain constant, they can be combined to yield a unified value.

$$F = \frac{Q}{d^2}$$

*Equation 2.2 Combined Strength Force*

The determination of  $Q$  can be accomplished through straightforward experimentation involving measuring the force of repulsion ( $F$ ) and knowledge of the radial distance ( $d$ ). In scenarios involving magnets in a clutch or other instances of co-rotational magnets, numerical evaluation is typically employed to transform  $d$  into a more practical format. For example, let  $r_0$  represent the radial distance to the outer magnet and  $r_i$  denote the distance to the inner magnet. Additionally, let  $\theta$  denote the angle between the magnets is

$$d = \sqrt{[(r_0 - r_i \cos[\theta])^2 + (r_i \sin[\theta])^2]}$$

*Equation 2.3 Distance Between Magnets*

This gives the radial and tangential force components

$$F_r = F \cos\phi \qquad F_t = F \sin\phi$$

*Equation 2.4* Radial and Tangential Force Components

The torque would be the tangential component of the force times the radius out to the hull.

$$T = F_t \frac{(r_o + r_i)}{2}$$

*Equation 2.5* Rotor Torque

Unlike point magnets, our magnetic clutch features discrete magnets, rendering the aforementioned analysis an approximation. While computational techniques capable of handling finite magnets exist, they fall beyond the purview of this research endeavor.

### CHAPTER 3

#### DESIGN AND FABRICATION OF A PROTOTYPE

The thruster is tailored for a compact autonomous underwater vehicle (AUV), designed to be portable and easily handled by a single operator. This requirement dictated that all aspects of the development had to be on a smaller scale, precluding the incorporation of any bulky components. As the vehicle is intended to operate at a leisurely pace, employing a propeller with a low rotational speed, the thruster's components were meticulously chosen to align with this criterion. Wherever feasible, the design aimed to integrate off-the-shelf components to streamline the construction process. Numerous experiments were conducted involving various magnet shapes and arrangements to refine the design concept. The final iteration of the design is depicted in Figure 3.1.

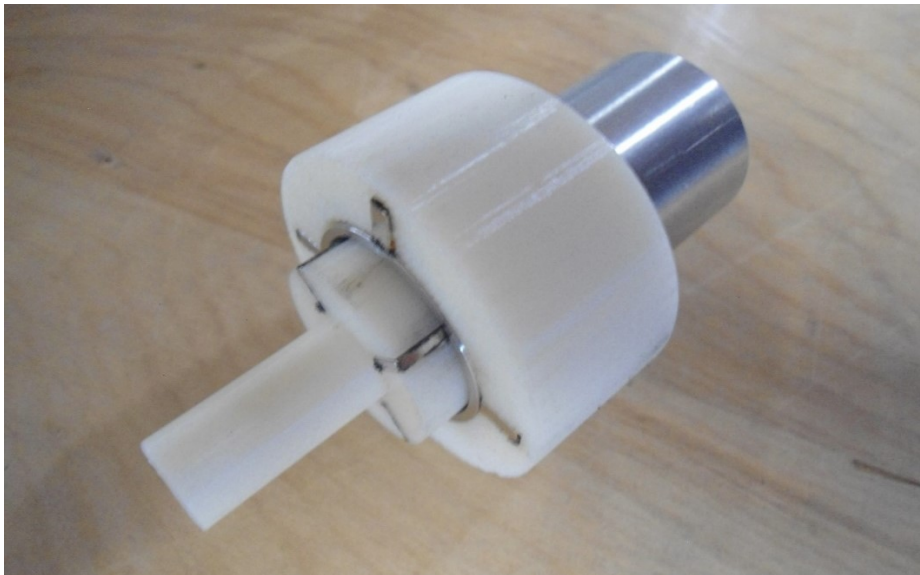


*Figure 3.1* Magnetic Clutch Arrangement

The design of the inside and outside magnet holders is shown in Figure 3.2 below.

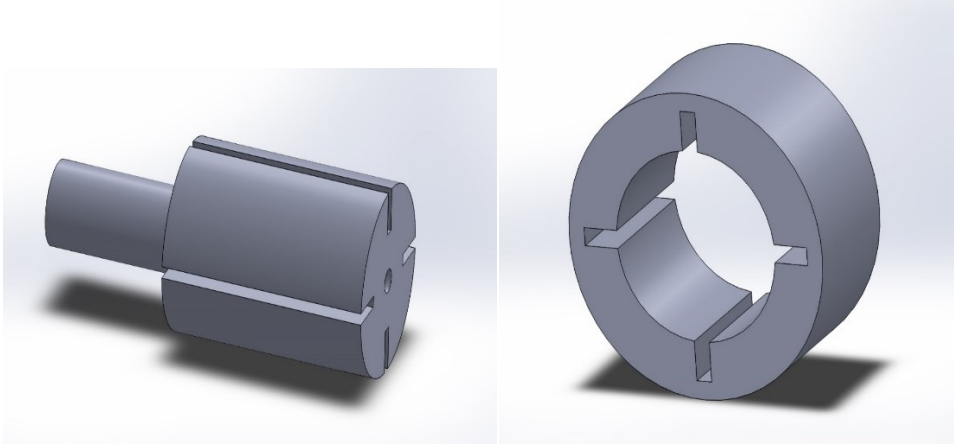


*Figure 3.2 Magnetic Clutch Arrangement CAD*



*Figure 3.3 Magnetic Clutch Arrangement*

The shaft of the clutch component, housed within the hull, is linked to the motor shaft, facilitating interaction between magnets when in close proximity. The length of the inner clutch shaft is carefully designed to minimize interference with the motor magnets. The propeller is affixed to the external component through a press-fit mechanism. Each component's magnets are magnetized radially, facilitating interaction along their edges. As the magnets within the hull possess identical polarity, they repel each other, providing a kind of radial bearing. Notably, the

neutral position between two objects is at 45 degrees, while the inner magnets maintain a neutral axial position relative to the outer magnets, resulting in an axial bearing effect. The clutch's geometry permits the incorporation of additional magnets if required.

The magnets used in this project were procured from K&J Magnetics and are classified as Neodymium (NdFeB) Magnets. Renowned for their exceptional strength, Neodymium magnets are considered the most potent type of permanent magnets accessible in the commercial market (K. J. Magnetics, n.d.). Their unparalleled magnetic strength and reliability make them an ideal choice for applications requiring high performance and efficiency.



*Figure 3.4 Neodymium Magnets*

For the drive, a 1" diameter geared brushed DC motor was selected. Geared motors offer higher torque compared to straight- drive motors and operate at slower speeds, making them suitable for this application. The increased torque provided by the geared motor ensures its capability to overcome the hydrodynamic torque generated by the rotating propeller. Utilizing equipment from the previous unit, the geared DC brush motor was chosen for its affordability, simplicity, and extended lifespan in challenging operating conditions compared to brushless



motors. Additionally, opting for a DC motor over an AC motor was preferred to minimize complexity and leverage existing battery resources. It is important to note that although a DC power supply was used for the tests, the batteries are not included in this project.



*Figure 3.5 Geared DC Brush Motor*

A motor holder was developed that allowed easy access to the motor wires.

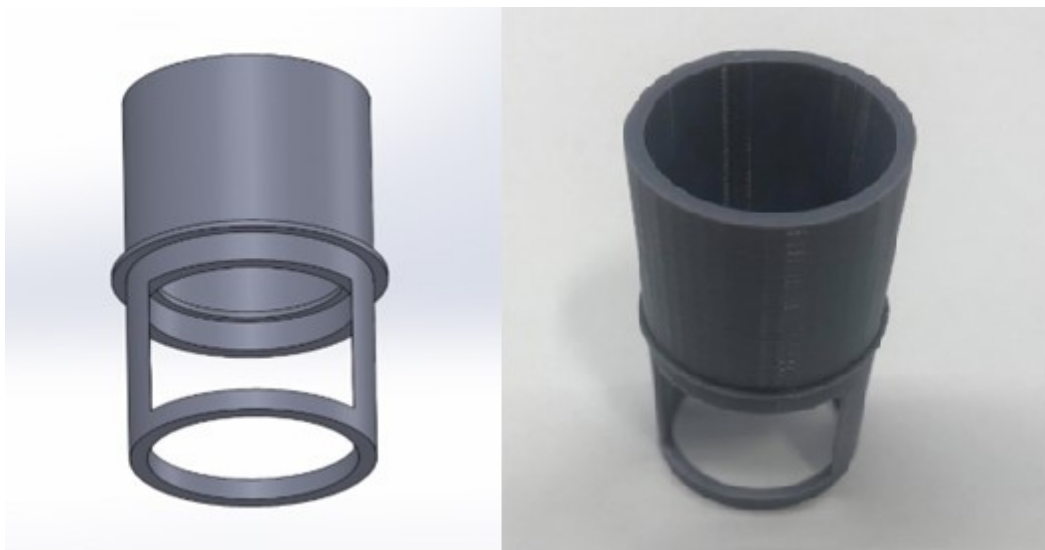


*Figure 3.6 DC Motor Holder*

The thruster's hull is required to endure the hydrostatic pressure encountered during submersion, necessitating the use of nonmagnetic materials to prevent the clutch components from adhering to it. Additionally, the hull should possess a thin wall thickness to enable close interaction between the clutch components. After careful consideration, a stainless steel pipe with a 1/8" wall thickness and a diameter slightly larger than 1" was selected as the optimal choice for the hull.

To ensure non-magnetic properties and adequate size to accommodate the DC motor, a stainless steel pipe was procured from McMaster-Carr facilitated by Dave Snook from Tech Services (McMaster-Carr. (n.d.)). This selection fulfills the requirement of a non-magnetic material for the hull while providing sufficient space for the motor's installation.



*Figure 3.7* Stainless Steel Pipe

The hull tube is subjected to external hydrostatic pressure, resulting in compressive hoop stress on its wall. Basic calculations indicate a maximum water depth tolerance of approximately 3211 m, as detailed in Appendix F. Considering the maximum depth of our AUV of about 100 m, this results in a safety factor of 32.

To waterproof the interior of the pipe and minimize drag, end caps were designed to be flush with the top components. Due to potential porosity issues with certain 3D-printed plastics, manual machining was deemed necessary for the end caps. This required simple machining techniques. While a shape without sharp edges would be optimal for drag reduction, the complexity led to the selection of a cone-like design with flat ends to accommodate O-rings. These end caps were tightly fitted over the pipe, with O-rings added to the interior of each for waterproofing. Additionally, an O-ring plug was incorporated at the back for wiring connections, while a screw with an O-ring was placed at the front to facilitate air escape during assembly. These delrin end caps with O-rings were used to complete and seal the hull.



*Figure 3.8 Delrin End Caps with O rings*

For the plug, we used a waterproof subcon connection. To wanted to utilize a more quick connection assembly early on in the project development but were unable to find a suitable connection that would meet our size requirements and budgetary cost.



*Figure 3.9* Waterproof Subcon Connection

The propeller has been precisely fitted in a way to press fit onto the outer magnet holder. To ensure balanced performance in both forward and reverse thrust, a propeller with matching characteristics for pitch and angle of attack was selected. This configuration is illustrated schematically in the figure below.

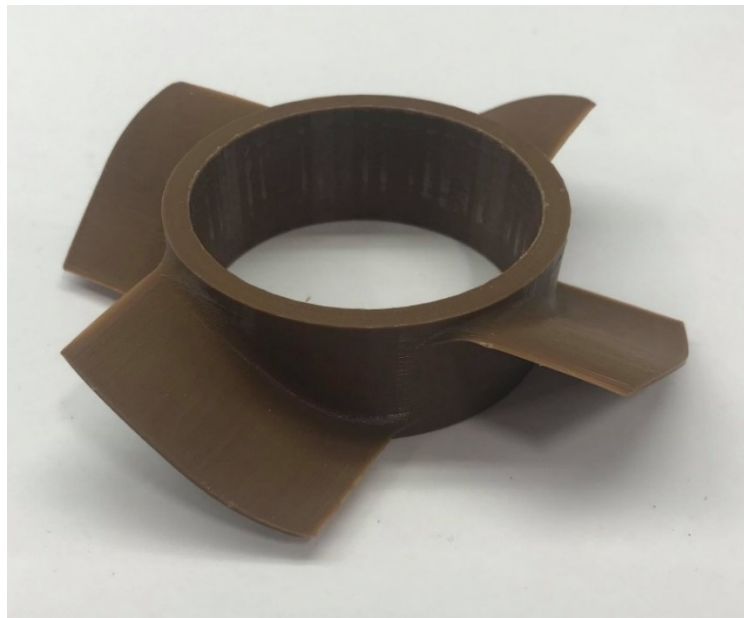


*Figure 3.10* 3D Printed Propeller

Adhering to industry standards, the four-fin model was adopted, leading to multiple iterations in designing the fins for the propeller. It was engineered to seamlessly press-fit onto the output shaft, facilitating easy replacement if task-specific variations were required.

The rotation around an axis induces airflow over the propeller blade, creating a pressure differential between its surfaces, thus generating lift. At the blade tip, this pressure variance triggers a flow from the high-pressure side to the low-pressure side, intertwining with the axial flow to form a vortex. The vortex's kinetic energy, sourced from the blade, contributes to drag. As both high and low pressure diminish at the tip, there is a consequent reduction in lift.

To mitigate thrust loss stemming from tip vortices, a propeller shroud was developed to obstruct airflow and enhance lift. The propeller resides within this shroud or duct, resembling a tube or tunnel. However, this design imposes a size restriction, as the blade diameter must not surpass the inner diameter of the duct. Despite this limitation, the duct offers the advantage of enhancing thrust efficiency for the same power input. Ordinarily, the duct's forward end has a larger diameter than its rear end. This configuration enables the propeller to continually draw water into the duct, subsequently expelling it through a narrower outlet. However, this feature was not considered, as the thruster was required to deliver uniform forward and reverse thrust. Additionally, a set screw hole was incorporated into the shroud to prevent rotation.

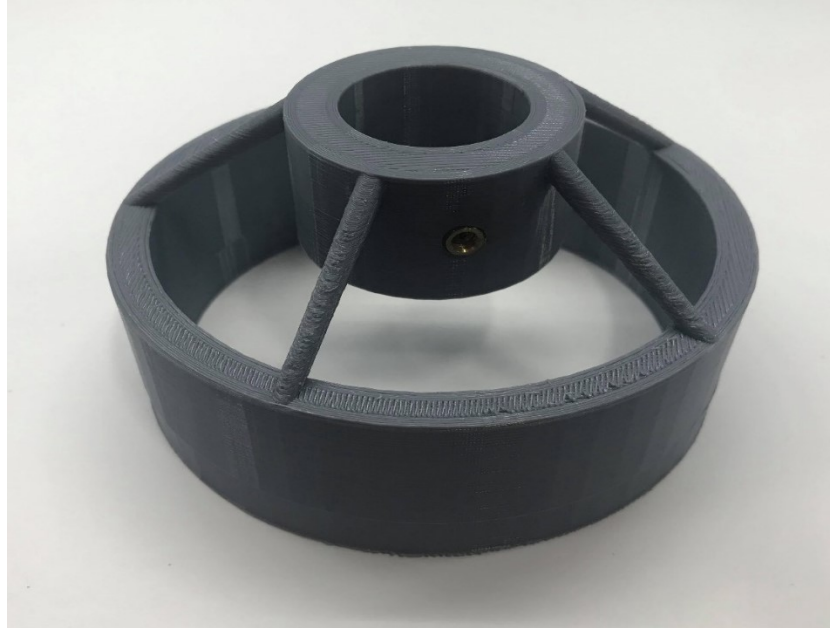


*Figure 3.11 3D Printed Shroud*

A hydrodynamic thrust bearing was utilized to facilitate the axial positioning of the propeller. This bearing comprises a single, immobile disc with radially cut grooves along its surface, dividing it into distinct land surfaces. These grooves serve as channels for the lubricant flow between the bearing and the thrust collar. As the thrust collar rotates against the bearing, the lubricant within the grooves is evenly distributed across the contact surface of the bearing. Unlike conventional flat land bearings, our design incorporates a step jump on the land, wherein there is a transition from one constant level to another. Appendix D provides theoretical insight into this configuration. According to the pressure gradient equation, gradients remain constant within regions with consistent gaps, resulting in a linear pressure variation within these areas. When the distance between the step and the opposing surface diminishes sufficiently, thrust equilibrium is achieved.



*Figure 3.12* Hydrodynamic Bearing

The hydrodynamic bearing was crafted from Rulon, chosen for its exceptionally low friction coefficient among materials. Sourced from McMaster-Carr, it underwent modifications with the aid of Tech Services to suit our specific requirements. Additionally, a spacer was fabricated to occupy the space between the other components, ensuring their stability. Two spacers were produced—one for the thruster and another shorter one designed to accommodate the attachment of an arm for testing purposes.

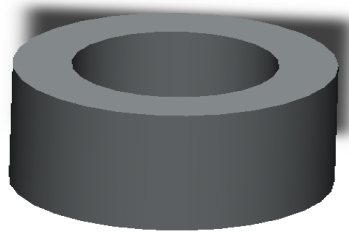


*Figure 3.13* General Spacer CAD Model

A schematic of the final design is shown in Figure 3.14.

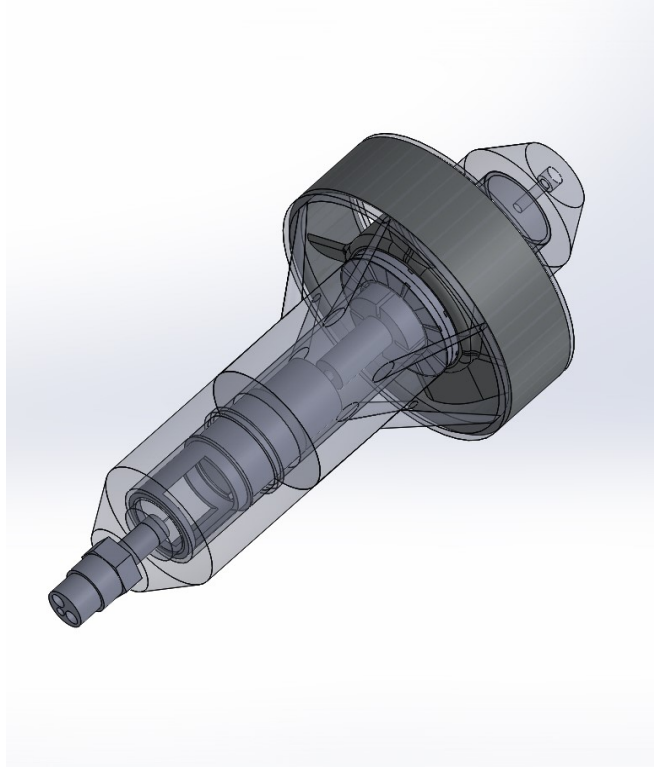


*Figure 3.14* Final Thruster Schematic

A photo of the final design is shown in Figure 3.15.



*Figure 3.15* Fabricated Prototype



## CHAPTER 4: TESTING OF THE THRUSTER

The composition of an underwater thruster's numerical framework hinges entirely on the electric motor's performance output. The thrust force is contingent upon various factors, including the motor model, propeller specifications, and other variables, rendering the creation of a mathematical model highly intricate. Thus, to circumvent this complexity, a precise identification approach is essential, necessitating the construction of the model through bench testing to gather input-output data. As outlined by Guibert (2005), the industry standard for conducting such bench tests involves the utilization of a water-filled test tank, the propulsion system comprising the motor and propeller, an instrument for thruster control, and a method for measuring requisite physical quantities.

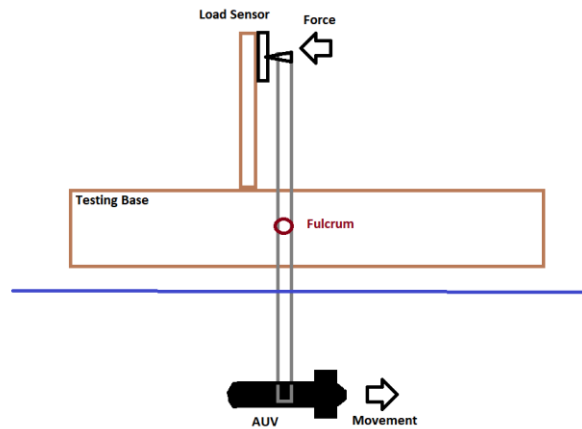


*Figure 4.1* Bench Test Set Up

### Fabrication of Test Frames

The design, inspired by the approach used by the Dynamical System and Control Laboratory (DSCL) as outlined by Whitcom & Yoerger (1999), includes a specific setup for the

evaluation of AUV thrusters. Initially, a tank equipped with a fixed horizontal support structure consisting of overhanging wooden beams is required. Attached to this structure is a vertical beam that pivots, securely holding the AUV thruster within the tank. At the opposite end of this beam, which remains above the water, a force sensor is strategically positioned. This sensor, placed at an equal distance from the pivot as the thruster, accurately measures and relays the thrust generated by the AUV thruster. This setup ensures precise measurement of the thruster's performance, which is crucial for assessing and enhancing AUV functionality.

### **Description of the Bench Test**

The aim of this project was to develop a test bench capable of evaluating and validating the concept of a newly designed underwater thruster intended for future integration into an underwater vehicle. The design requirements for this test bench were multifaceted and included the following key aspects:

- The test bench needed to be sensitive enough to measure low force levels accurately. This necessitates a design that can not only capture subtle variations in thrust but also includes a system to digitize these measurements for precise analysis and record-keeping.
- The structure of the test bench had to be compatible with the existing deep tank in the fluids lab. It was essential for the design not to interfere with the tank's water flow. This requirement implied that the test bench should be relatively simple to construct yet effective in its purpose. Moreover, it needed the capability to measure thrust in both directions, which adds a layer of complexity to its design.
- The test bench design should allow for the easy mounting of the thruster. It was crucial that this integration did not significantly impact the thruster's own design or functionality. This requirement speaks to the need for a flexible and adaptable mounting system that can

accommodate the thruster without necessitating major modifications to either the thruster or the test bench.

### **Description of the Bench Test**

The foundation of this setup is a tank that serves as a controlled environment for testing the AUV thruster. The tank should be large enough to accommodate the thruster and the apparatus, allowing for free movement and accurate measurement. The size of the tank is crucial as it needs to simulate, as closely as possible the conditions the AUV would be exposed to in open water. For this project, we used the deep testing tank located in the fluids lab, which is more than adequate.

### **Horizontal Support Structure**

Overhanging wooden beams form a crucial part of the horizontal support structure. These beams need to be sturdy and well-anchored to provide stability to the entire structure. The support is built from 2x4 in wooden joints fixed across the tank, both horizontal and one vertical. The material (in this case wood) should be selected for its durability and water resistance to ensure longevity and reliability under repeated testing.

### **Vertical Beam with Pivot Connection**

The design incorporates a vertical beam, hinged to a horizontal support, which serves a critical function in securely holding the AUV thruster inside the tank. This hinged or pivoted arrangement of the beam provides a range of motion, effectively simulating the diverse angles and orientations an AUV thruster might experience in actual underwater conditions. The engineering of the pivot is key, ensuring it facilitates smooth movement while maintaining the

overall stability of the setup.

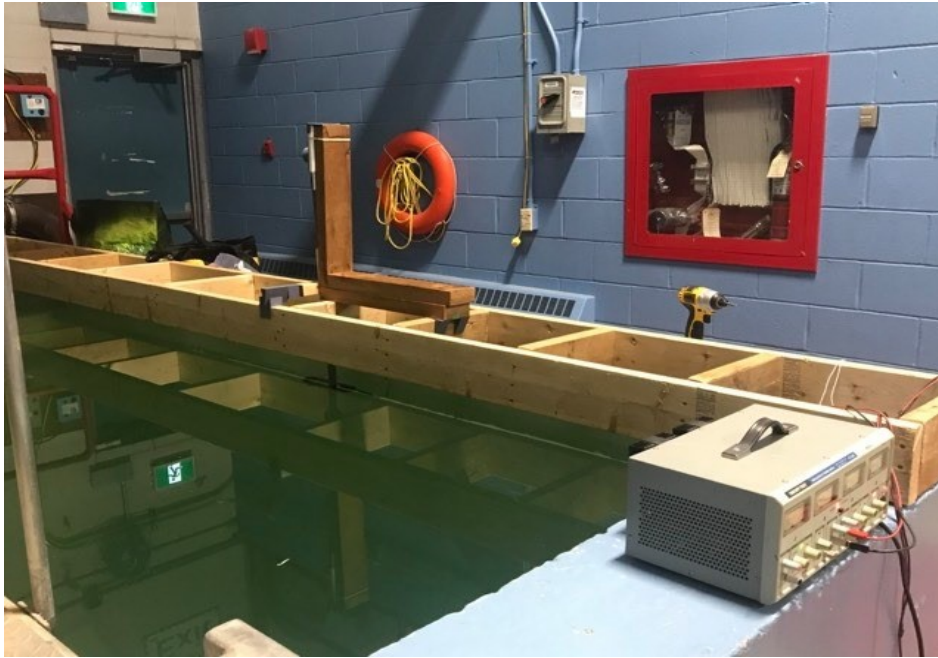


*Figure 4.2* Fluid Lab Deep Tank Set Up

In order to accurately measure the thrust force generated by the AUV thruster, a cross-patterned balance mechanism resting on knife edges is employed. This mechanism effectively transfers the force exerted by the thruster to the force sensor, which is strategically positioned above the tank. The use of knife edges is a highly recognized method for achieving precise geometrical constraints, crucial for the accurate placement and fine-tuning of the components. This setup is not only essential for ensuring precise location but also plays a pivotal role in comparing fundamental standards of mass, enhancing the overall accuracy and reliability of the thrust measurement process.

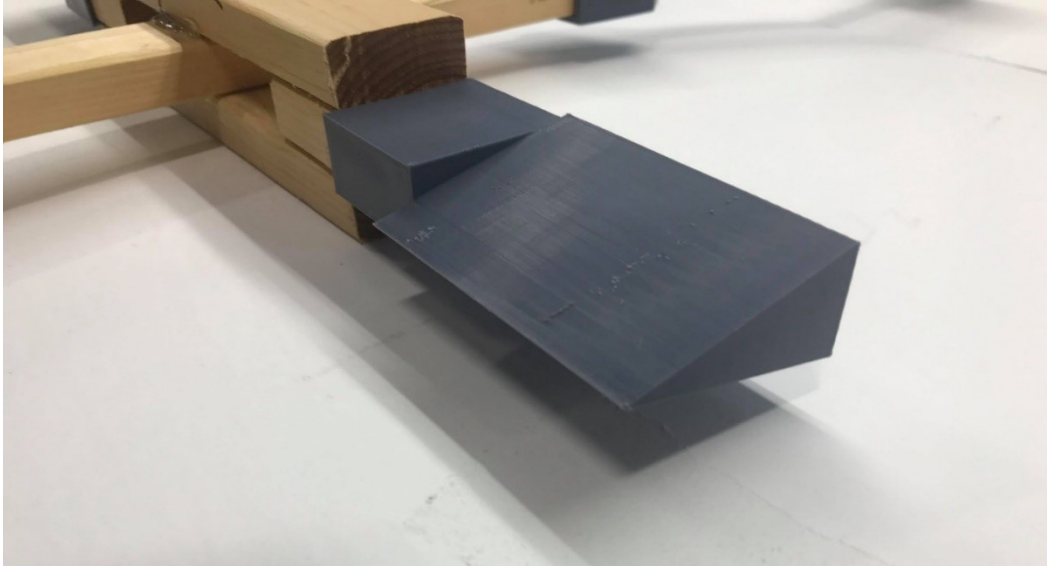


*Figure 4.3 Knife Edge Fulcrum*

## **Electronics**

A load cell from a Kitchen food scale is used to measure the thrust force generated. It has been verified to read accurately in grams and gives measurable data to 0.001 grams.



*Figure 4.4 Electronic Scale*

A precision power supply was used to drive the motor.



*Figure 4.5 Power Supply*

## **Load Frames**

Attaching the thruster to the testing unit requires a method that minimizes currents and interference. The arms of the balance were designed to be the same length in order to balance the moment forces and are attached behind the flow in place of the spacer so as not to impede the water's entry into the duct. The arms at the end of the wooden cross were 3D printed and attached with hot glue. This was done in the hope that the wooden cross could be replaced with a longer one to adjust the unit's depth in the water, but this was no longer necessary due to the ability to raise the water level. In addition, the arms were printed to the maximum length of the 3D printer for one part at a time.

Using an adapter for the testing apparatus that held the unit on its side restricted forward motion and only allowed the thruster to be affected by the generated torque force. The horizontal force generated by the torque created was recorded. This was also tested in two different

positions to ensure repeatability. These were used in our results, but it is important to note how they contribute to the validation of the setup.

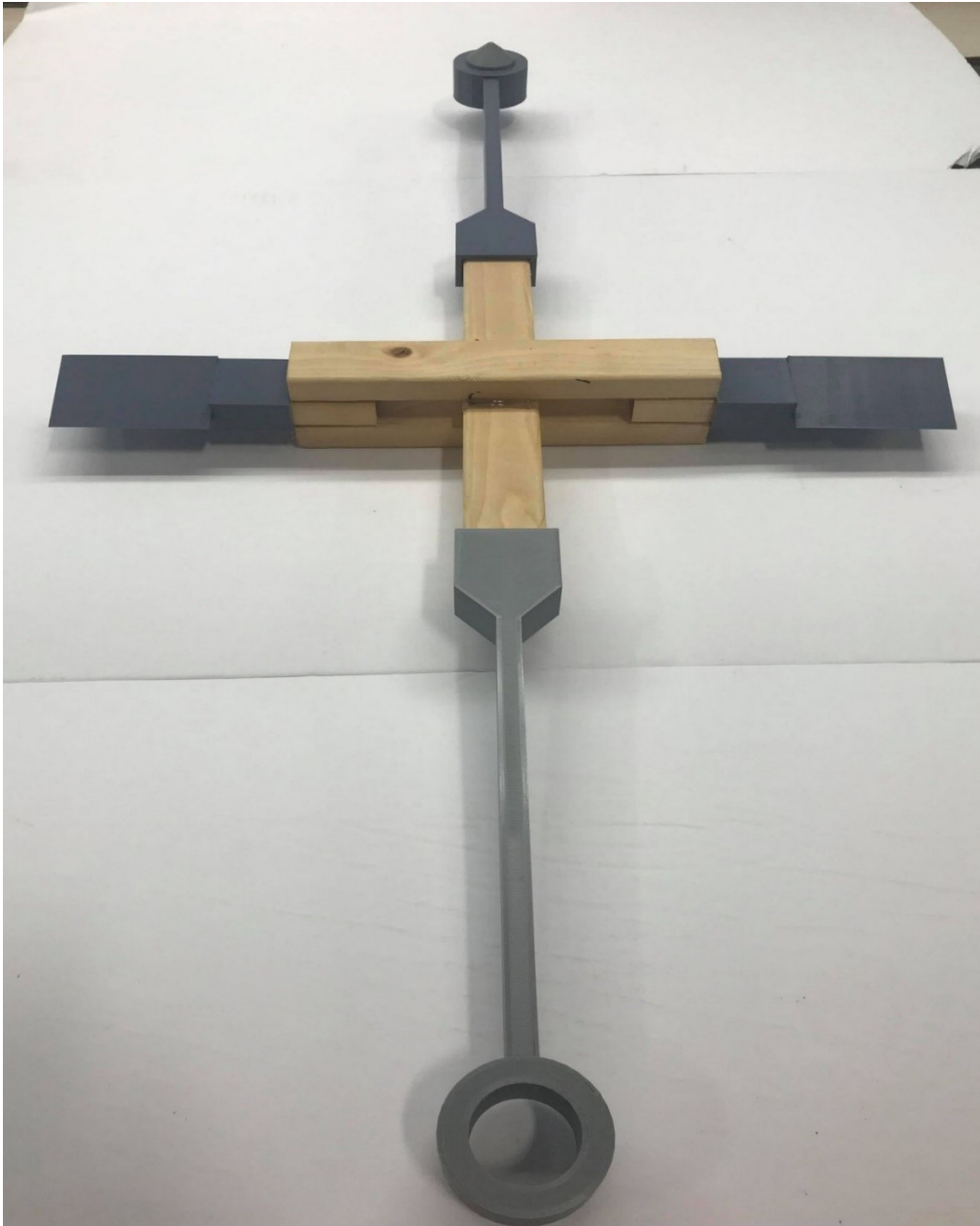


*Figure 4.6* Thrust Frame



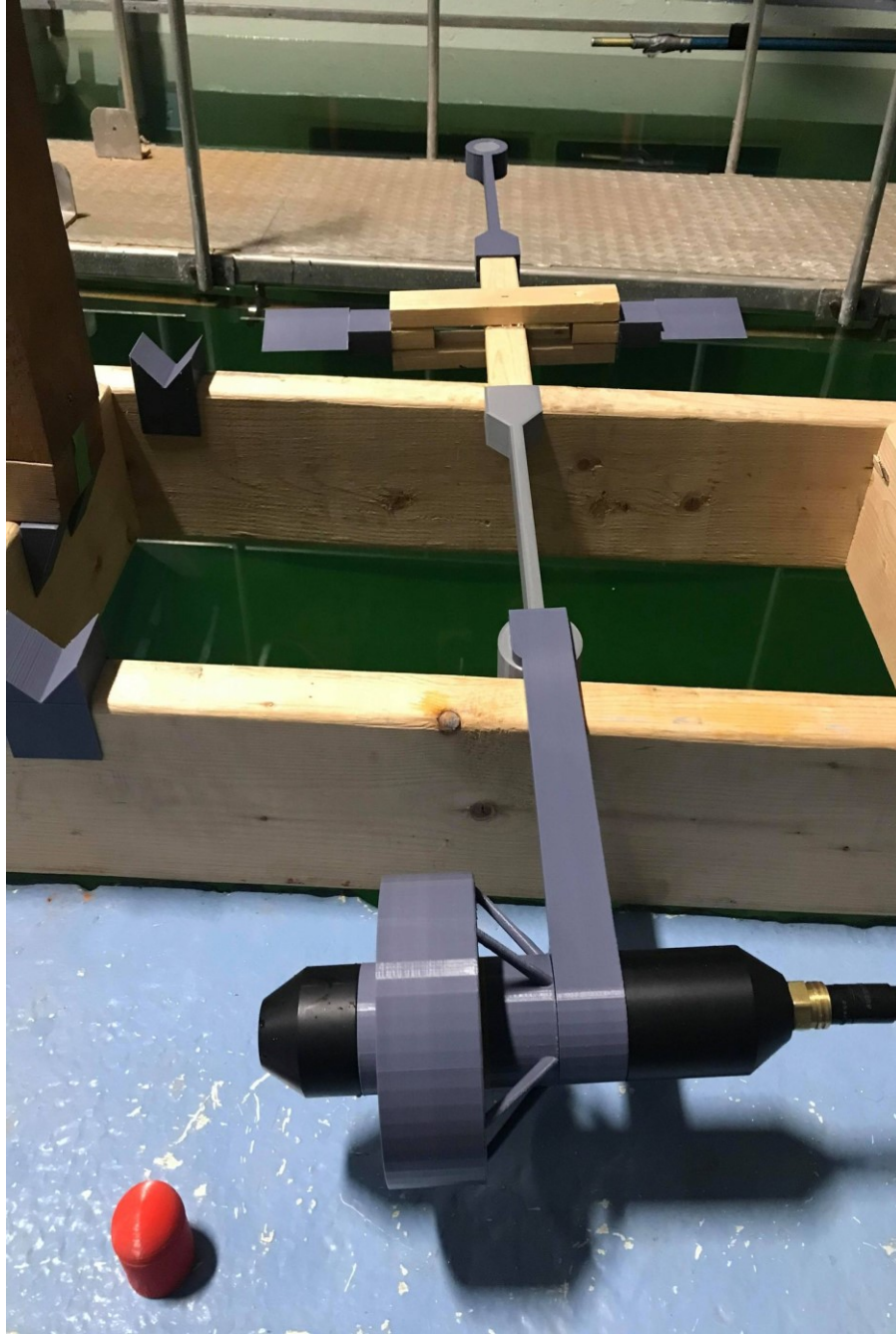


*Figure 4.7 Torque Frame*



## Test Results

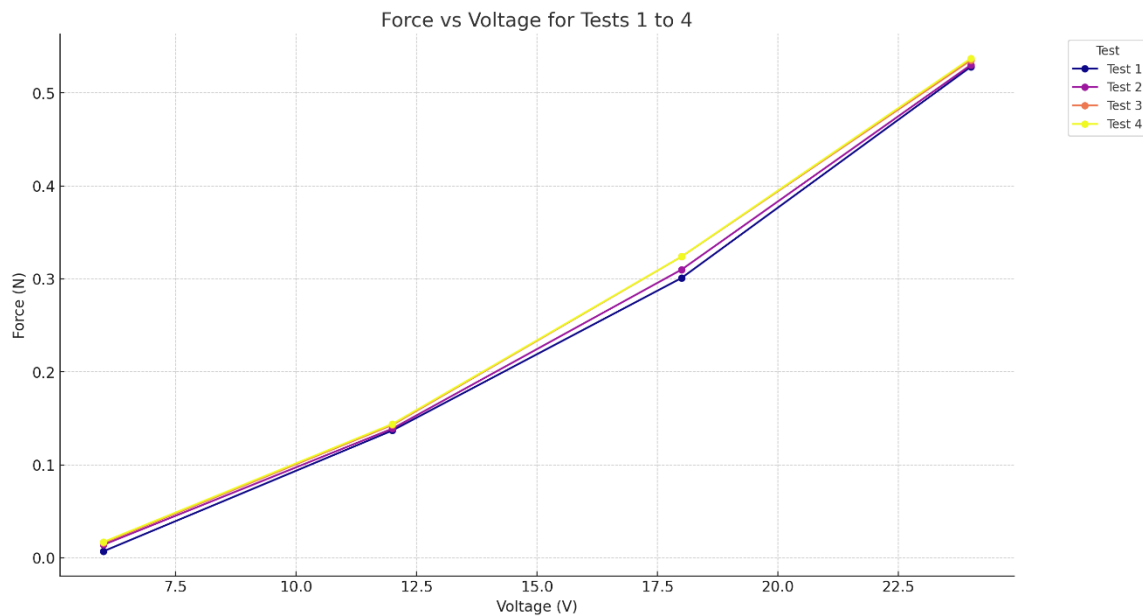
The setup was subjected to nine tests. Thrust was the primary data recorded. Raw data from these tests can be found in Appendix B. Except for the sixth test, all tests used a shroud. In the fifth test, the motor was operated in reverse. In the sixth test, the duct was removed. In the seventh and eighth tests, the rotational torque was measured. Measurement of force was measured using the weight in grams and converted into force using Newton's Law.

*Table 4.1* Tank Depth and Wall Distance

Test	Depth	Wall	Load	Direction
1	Partly Submerged	>5ft	Thrust Shroud	Forward
2	Fully Submerged	>5ft	Thrust Shroud	Forward
3	4 inches deep	>5ft	Thrust Shroud	Forward
4	8 inches deep	>5ft	Thrust Shroud	Forward
5	8 inches deep	>5ft	Thrust Shroud	Reverse
6	8 inches deep	>5ft	Thrust No Shroud	Forward
7	8 inches deep	8 inches away	Torque Shroud	Forward
8	8 inches deep	>5ft	Torque Shroud	Forward
9	8 inches deep	>5ft	Thrust Shroud	Forward

## Difference Caused by Submerged Level

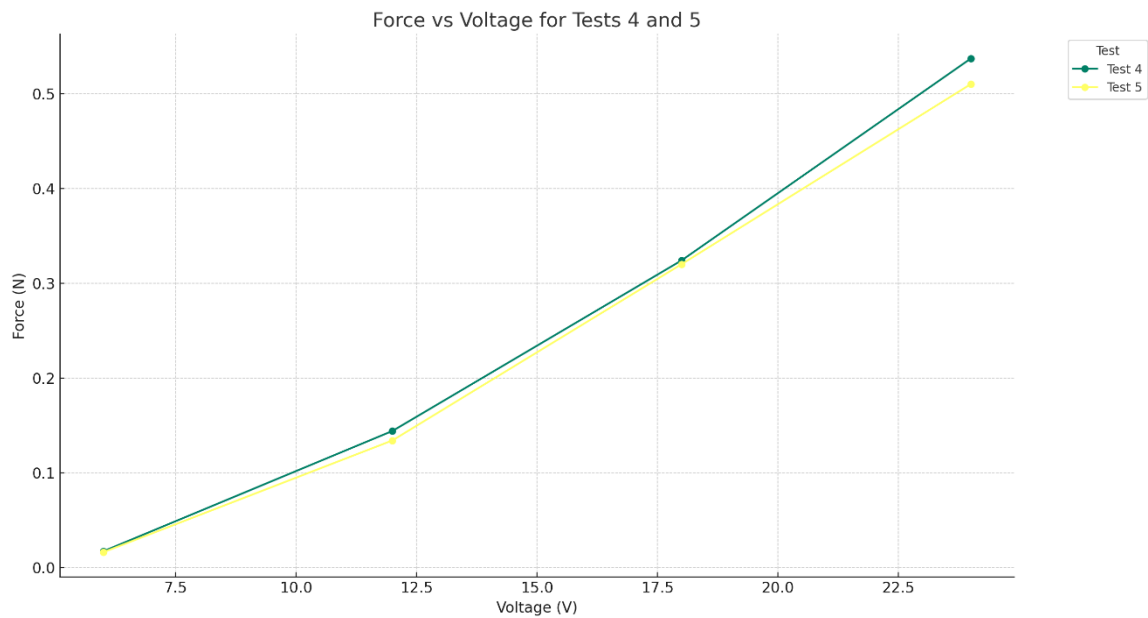
Upon analyzing the data recorded at various depths, two significant findings emerge. Initially, the repeatability of test outcomes is apparent. This is evidenced by the graph, which shows a striking consistency in the data recorded across different tests, indicating a high level of reliability in the thruster's performance. The marginal differences observed suggest an operation largely unimpeded by external factors. Additionally, the thruster's force generation appears to be constant at different depths under full submersion, in contrast to the observable losses when partially submerged.



*Graph 4.1* Difference Caused by Submerged Level Graph

## Difference of Forward and Reverse

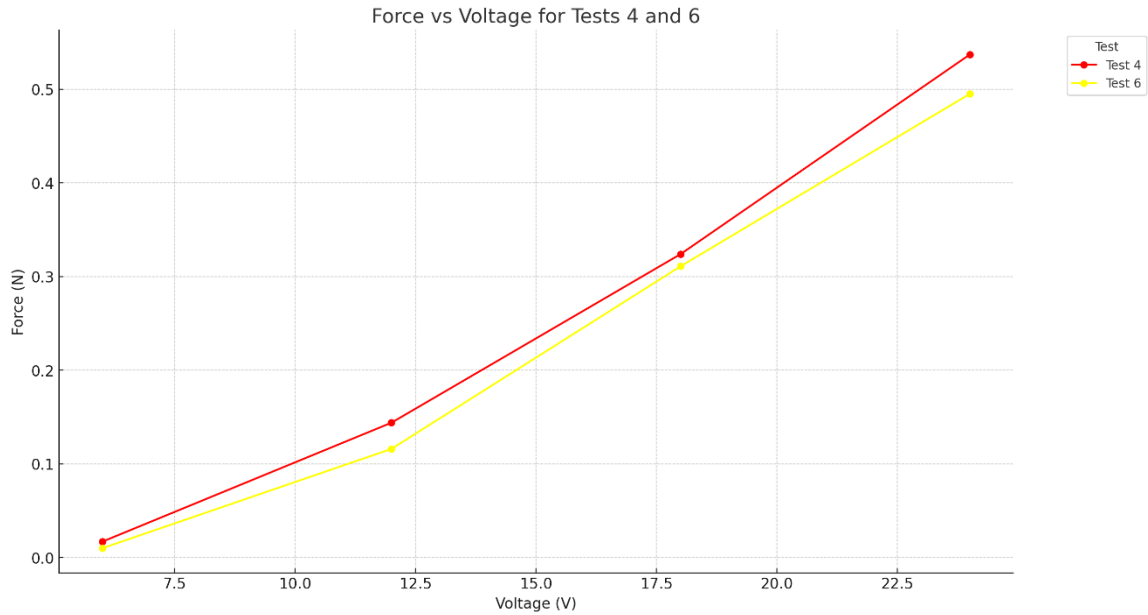
Analysis of the data indicates not only repeatability, but also a minor difference between the generated thrust in forward and reverse directions. The slight decline in reverse thrust is linked to the interference caused by the test structure's holder. Although this holder is optimized to minimize the loss in forward thrust, it inadvertently impacts the reverse thrust. In reverse, the bar, located at the forefront of the flow, is inadvertently drawn into the duct, resulting in a modest force reduction.



*Graph 4.2* Difference of Forward and Reverse Graph

## Duct Efficiency

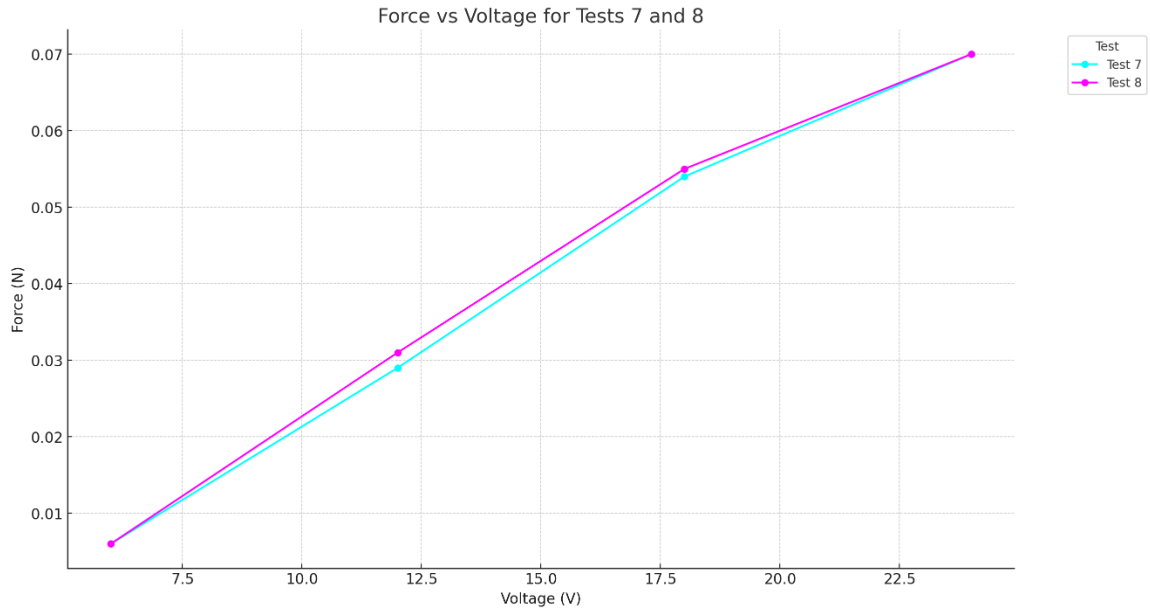
In alignment with earlier predictions and detailed discussions, it is evident that the duct contributes to an increased power generation by the thruster. Future investigations should delve deeper into this aspect, exploring potential enhancements to capitalize on this effect further.



*Graph 4.3 Duct efficiency graph*

## Torque Output

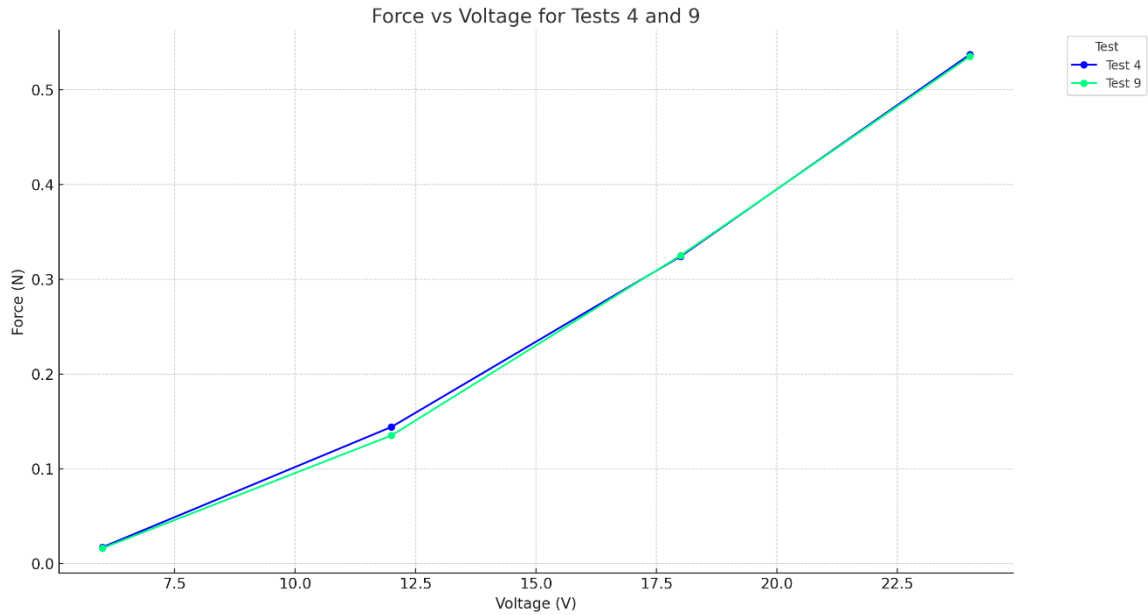
Analysis of the graph, which depicts the torque load generated by the thruster against the applied voltage, indicates that wall interference does not skew the data, thus supporting the repeatability of our findings. The trend across the tests displayed a similar, almost linear increase. This consistency is crucial, as there is virtually no significant discrepancy between the test outcomes. However, the graph reveals a diminishing steepness as the input voltage approaches the maximum capacity of the motor.



*Graph 4.4 Torque output graph*

### Wall Interference

In the graph portraying the thruster's forward force against applied voltage, both tests parallel each other, displaying an upward trajectory without significant deviation. This uniformity underlines the absence of wall interference, thus bolstering the argument that our data could be reflective of open water conditions.



*Graph 4.5 Torque output graph*

## **Proof Of Concept**

This project was undertaken to assess the effectiveness of our novel thruster concept, which incorporates a magnetic clutch to create torque specifically designed to counteract external frictional forces from propeller configurations and water dynamics.

Our thorough analysis of the data has led to several important conclusions. First and foremost, the design's ability to generate a strong and effective propulsion force fulfills our primary objective and represents a solid achievement in thruster development. The data also shows remarkable consistency, indicating minimal impact from external factors and suggesting the thruster's reliable performance in variable marine conditions. Additionally, the operational stability, demonstrated by the steady force output and lack of data irregularities, points to the magnetic bearings effectively reducing frictional forces, a notable improvement over traditional thruster systems.

Moreover, our tests on thrust versus voltage demonstrate that thrust is relatively unaffected by changes in the parameters we tested. This suggests that thrust is primarily influenced by the fluid dynamics near the propeller blades, which provides valuable insight into the operational principles of our thruster design.

## **CHAPTER 5:**

### **CFD VALIDATION**

#### **Overview of CFD**

Multiple CFD software packages can simulate propellers. Each is based on fluid flow partial differential equations. Each can manage turbulence using the concept of eddy viscosity. Included in the packages are ANSYS Fluent, ANSYS CFX, Flow3D, and OpenFoam. Both ANSYS and Flow3D are expensive commercial codes. ANSYS is available at MUN. Previously, we had access to Flow3D, but its license was not renewed. Because of its steep learning curve, ANSYS was not utilized in our project. Flow3D is highly intuitive. It is also customizable. It is the only CFD software that permits the movement of objects through the grid. We used it to examine the depth control of a basic AUV. OpenFOAM (which stands for "Open-source Field Operation and Manipulation") is a free, open-source CFD (OpenFOAM. (n.d.)). It offers numerous free tutorials for specific applications, including propellers. Due to this, the software OpenFoam was used. Additionally, the fact that it is free would facilitate future work.

#### **Governing Equations**

Typically, hydrodynamic flows are turbulent. They consist of numerous small eddies. The viscosity of a gas is a result of the random motions of its molecules, which diffuse momentum and give the gas its viscosity. Small eddies in a turbulent flow diffuse momentum, making the fluid appear more viscous than it is. This apparent increase in viscosity regulates the overall flow pattern and structural loads. Eddy viscosity models are the models that account for this noticeable increase in viscosity.

Conservation of mass considerations given for such flows:



$$\frac{\partial P}{\partial t} + \rho c^2 (\frac{\partial U}{\partial x} + \frac{\partial V}{\partial y} + \frac{\partial W}{\partial z}) = 0$$

*Equation 5.1 Conservation of mass*

Where U V W are fluid velocities, P is pressure,  $\rho$  is fluid density, and c is the speed of sound in water. Although water is basically incompressible, for mass conservation, CFD takes it to be compressible.

Conservation of momentum considerations give:

$$\rho (\frac{\partial U}{\partial t} + U\frac{\partial U}{\partial x} + V\frac{\partial U}{\partial y} + W\frac{\partial U}{\partial z}) + A = -\frac{\partial P}{\partial x} + [\frac{\partial}{\partial x} (\mu\frac{\partial U}{\partial x}) + \frac{\partial}{\partial y} (\mu\frac{\partial U}{\partial y}) + \frac{\partial}{\partial z} (\mu\frac{\partial U}{\partial z})]$$

$$\rho (\frac{\partial V}{\partial t} + U\frac{\partial V}{\partial x} + V\frac{\partial V}{\partial y} + W\frac{\partial V}{\partial z}) + B = -\frac{\partial P}{\partial y} + [\frac{\partial}{\partial x} (\mu\frac{\partial V}{\partial x}) + \frac{\partial}{\partial y} (\mu\frac{\partial V}{\partial y}) + \frac{\partial}{\partial z} (\mu\frac{\partial V}{\partial z})]$$

$$\rho (\frac{\partial W}{\partial t} + U\frac{\partial W}{\partial x} + V\frac{\partial W}{\partial y} + W\frac{\partial W}{\partial z}) + C = -\frac{\partial P}{\partial z} - \rho g + [\frac{\partial}{\partial x} (\mu\frac{\partial W}{\partial x}) + \frac{\partial}{\partial y} (\mu\frac{\partial W}{\partial y}) + \frac{\partial}{\partial z} (\mu\frac{\partial W}{\partial z})]$$

*Equation 5.2 Conservation of momentum*

Where  $\mu$  is the effective viscosity of the water and A B C are turbulence source terms. The effective viscosity comprises laminar viscosity and an eddy viscosity due to turbulence. Here, this is given by the  $k\epsilon$  turbulence model, where k is the kinetic energy of turbulence and  $\epsilon$  is the dissipation rate of turbulence. Its governing equations are:

$$\frac{\partial k}{\partial t} + U\frac{\partial k}{\partial x} + V\frac{\partial k}{\partial y} + W\frac{\partial k}{\partial z} = T_P - T_D + [\frac{\partial}{\partial x} (\alpha\frac{\partial k}{\partial x}) + \frac{\partial}{\partial y} (\alpha\frac{\partial k}{\partial y}) + \frac{\partial}{\partial z} (\alpha\frac{\partial k}{\partial z})]$$

$$\frac{\partial \epsilon}{\partial t} + U\frac{\partial \epsilon}{\partial x} + V\frac{\partial \epsilon}{\partial y} + W\frac{\partial \epsilon}{\partial z} = D_P - D_D + [\frac{\partial}{\partial x} (\beta\frac{\partial \epsilon}{\partial x}) + \frac{\partial}{\partial y} (\beta\frac{\partial \epsilon}{\partial y}) + \frac{\partial}{\partial z} (\beta\frac{\partial \epsilon}{\partial z})]$$

*Equation 5.3 Governing Equations of  $k\epsilon$  Turbulence Model*

Where the T D terms account for the production and dissipation of turbulence.

A special function  $F$ , known as the volume of fluid or VOF function, can be used to locate the water surface. For water,  $F$  represents unity; for air, it is assumed to be zero. Regions with  $F$  between unity and zero must contain the water surface. Material volume considerations are given as follows:

$$\frac{\partial F}{\partial t} + U\frac{\partial F}{\partial x} + V\frac{\partial F}{\partial y} + W\frac{\partial F}{\partial z} = 0$$

*Equation 5.4 Material Volume*

For CFD, each PDE is put into the form:

$$\frac{\partial M}{\partial t} = N$$

*Equation 5.5 Partial Differential Equation for CFD*

Within each CFD cell, each governing equation is integrated numerically across a time step to get:

$$M(t+\Delta t) = M(t) + \Delta t N(t)$$

*Equation 5.6 Time Stepping Scheme*

Current values in cells are used to approximate the terms of the spatial derivative in  $N$  for each cell. The momentum equations are used to update  $U V W$ , the mass equation is used to update  $P$  and correct  $U V W$ , and the turbulence equations are used to update  $k$  and  $\varepsilon$ .

## **OpenFOAM CFD**

OpenFOAM is a collection of open- source libraries and applications. Foam in OpenFoam refers to a namespace for a dialect of C++ and has nothing to do with fluid. This C++ toolbox is used to develop customized numerical solvers and pre-/post-processing utilities for the solution of problems in continuum mechanics. Solvers, which are CFD applications are included. It contains numerous tutorials, mainly created by users. This project was inspired by a tutorial titled "Propeller"

OpenFoam can manage multiple flow types. In the current work, the solver is used for an incompressible and viscous fluid. The governing equations are mass conservation and momentum conservation. To approximate the effect of turbulence, the  $k$ - $\varepsilon$  eddy viscosity model is applied.

The solvers are organized by topic, with Basic, HeatTransfer, Incompressible and Multiphase being the most common. Within these solvers you will typically discover a few general solvers and some of their derivatives (for example for dynamic meshes). Since we are dealing with steady-state incompressible flows (laminar and turbulent) of a single-phase fluid, the work focuses on the use of incompressible solvers for the simulation. This work employs a solver for an incompressible, viscous fluid. pimpleFoam was chosen over pisoFoam because the PIMPLE (merged PISO-SIMPLE) algorithm allows for a large time step (over a coronal number of one). The governing equations are mass conservation and momentum conservation. To approximate the effect of turbulence, the  $k$ - $\varepsilon$  eddy viscosity model is applied.

It works by doing the following four steps:

1. Pre-Processing: Creation of Geometry
2. Meshing: Dividing domain into tiny boxes called cells.
3. Solving: Calculating interaction between adjacent cells
4. Post-Processing: Collection and processing of results

This is detailed in detail in Appendix C.

### **CFD Results**

The Computational Fluid Dynamics (CFD) analysis detailed in this thesis took approximately one week to complete. The simulation was performed in incremental time steps, progressing from 0 to 2.5 seconds, then to 5, 10, and finally 20 seconds. Due to the frequent CFD simulation crashes, certain intervals necessitated repetition. These stepwise increments were essential, as achieving a quasi-steady thrust value demanded extended simulation time, likely attributable to the scaled-down numerical deep tank compared to its real-life counterpart. Our examination focused on a singular propeller subjected to CFD analysis at its maximal operational speed. This solitary data point sufficed to corroborate the experimental reliability and the effective functioning of the magnetic clutch. Additional data was deemed superfluous for this purpose.

Through CFD simulations, two principal data categories are computed: visual and numerical. The visual data elucidates the flow patterns initiated by the thruster, enabling precise flow dynamics analysis. Conversely, the numerical data quantitatively estimates the force generated. Employing CFD for force prediction facilitates direct comparison with the experimental outcomes from the concept model, serving as a critical validation step for the design. The simulation conspicuously illustrates the flow trajectories via streamlines. These

results are effectively visualized using a Graphical User Interface (GUI), specifically paraFoam, as exemplified below:

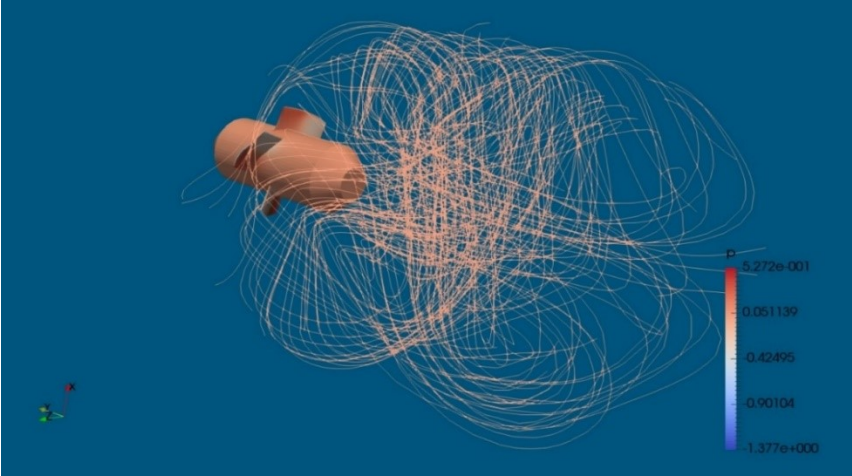
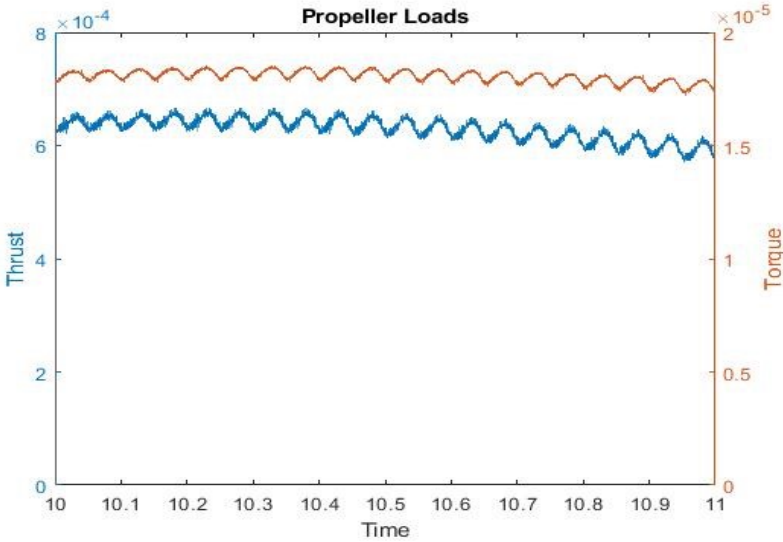


Figure 5.1 ParaFoam results

Results like propeller thrust versus time can be plotted in software such as MATLAB. An example is given below:



Graph 5.1 Thrust and Torque results

The derived CFD thrust from the sketch is roughly 0.0006 N, correlating to a specific density unit. For aquatic applications, the equivalent thrust scales to about 0.6 N – a thousandfold increase – equating to nearly 0.06 kilograms or 60 grams. Empirical measurements via a load cell echoed this figure, affirming a consistent thrust of approximately 60 grams. This congruence between CFD and experimental data is observed under conditions of 300 RPM propeller rotation, the motor's peak speed. A simplified propeller model presented in Appendix E approximates the thrust at 59 grams, aligning closely with both the CFD and experimental findings.

## **CHAPTER 6:**

### **CONCLUSIONS AND FUTURE WORK**

#### **Conclusions**

In summary, our project has successfully developed a magnetic clutch system that stands apart from existing larger models such as those from Tecnadyne. This achievement is primarily due to the fact that we opted for magnetic repulsion, moving away from traditional attraction-based methods that often require standard bearings. This strategic shift not only improved rotor efficiency but also reimaged the clutch as a radial journal bearing, making standard bearings redundant. Additionally, our innovative use of varying magnet lengths as an axial bearing emerged as a solution to alignment issues encountered with earlier designs.

The extensive testing carried out at MUN's Engineering Fluids Lab, using a carefully scaled model, has validated our design's functionality. These tests were not designed to compare with commercial models, but rather to demonstrate the effectiveness of our repulsion-based system and integrated axial bearing. The positive outcomes from these tests have been crucial in verifying that the clutch produces enough thrust for its intended purpose.

Moving forward, one could further refine our design by focusing on aspects such as propeller angles, duct design, material selection, and electrical components. This process would not just enhance the design, but also increase the overall performance to meet and exceed contemporary standards. The clutch's ability to maintain the input shaft's central alignment with minimal wear due to its non-contact nature is a notable feature of our design. These ongoing improvements will contribute significantly to the evolution of magnetic clutch technology, leading to more efficient, reliable, and effective solutions in the field.

## Future Work

While the data shows that this design is feasible, optimization of the thruster for any operation locations should be performed straightforwardly using the presented concept. Below are our recommendations for future work with regard to a specific task.

### Technical Improvements

- Enhancing Power Transmission
  - Increase the strength and number of magnets.
  - Modify the dimensions of the magnets for optimal power transmission.
- Development of a High Thrust, Low Torque Propeller
  - Design a propeller using OpenFOAM CFD analysis for reduced clutch strain.

### Numerical Analysis and Modeling

- Finite Element Analysis of the Magnetic Clutch
  - Develop a finite element model or find suitable existing software.
- Improved Magnet Interaction Modeling
  - Develop a line magnet model calibrated with test data.

### Material and Equipment Selection

- Selection of Motor and Bearings
  - Choose motor RPM and bearings based on speed requirements and ease of procurement.
- High-Grade Material Utilization
  - Use materials like carbon fiber for the propeller to suit force and depth requirements.



## Economic Feasibility

- Cost-Effectiveness Evaluation
  - Assess the financial viability for integration into other projects.

## Optimization Strategies

- Propeller and Duct Design Optimization
  - Determine optimal propeller angle of attack and duct sizing.
- Overall Conceptual Improvement
  - Continuous refinement to reach the full potential of the thruster concept.

## Practical Application and Testing

- Application in Autonomous Underwater Vehicles
  - Develop a magnetic clutch for real-world AUVs and test in marine environments.
- Corrosion Prevention
  - Implement protective coatings on external magnets to prevent seawater corrosion.

## REFERENCES

- Hinchey, M.J. (2016). *Undergraduate Fluid Mechanics Notes*. Mechanical Engineering Department, Memorial University of Newfoundland, Canada.
- Tecnadyne. (n.d.). *Tecnadyne: The Leader in Subsea Propulsion*. Retrieved July 4, 2020, from <https://tecnadyne.com/>
- McMaster-Carr. (n.d.). *McMaster-Carr - Catalog*. Retrieved March 22, 2011, from <https://www.mcmaster.com/>
- K. J. Magnetics. (n.d.). *K&J Magnetics - Strong Neodymium Magnets, Rare Earth Magnets*. Retrieved May 20, 2010, from <https://www.kjmagnetics.com/>
- Guibert, C. (2005). *Modélisation et commande en puissance de moteurs à courant alternatifs en propulsion navale*. Ph.D. thesis, University of Nantes
- Whitcomb, L.L., Yoerger, D.R., & Singh, H. (1999). *Advances in Doppler-based navigation of underwater robotic vehicles*. Proceedings 1999 IEEE International Conference on Robotics and Automation (Cat. No.99CH36288C), 1, 399-406 vol.1.
- OpenFOAM. (n.d.). *OpenFOAM is the free, open-source CFD software developed primarily by OpenCFD Ltd*. Retrieved May 11, 2020, from <https://www.openfoam.com/>
- 123seminaronly (n.d.). *Magnetic Bearings*. Retrieved Jan 7, 2021, <http://www.123seminaronly.com/Seminar-Reports/049/65784625-Magnetic-Bearing.doc>
- Mark D. Hinkley (Dec 17 2011). *Pumps and systems - The Attraction of Magnetic Bearings*. Retrieved Jan 13, 2021, <https://www.pumpsandsystems.com/attraction-magnetic-bearings>
- Xiang, X., Niu, Z., Lapierre, L., & Zuo, M. (2015). *Hybrid underwater robotic vehicles: the state-of-the-art and future trends*. *Hkie Transactions*, 22(2), 103-116

Navy. (Feb 05, 2021.). *Naval Technology - Mine Countermeasures Ships*. Retrieved July 01, 2011, from <https://www.navy.mil/Resources/Fact-Files/Display-FactFiles/Article/2171622/mine-countermeasures-ships-mcm/>

Monterey Bay Aquarium Research Institute. (n.d.). *MBARI – Research Vessel Western Flyer*. Retrieved July 01, 2011, from <https://www.mbari.org/at-sea/ships/research-vessel-western-flyer/>

Vokoun, D., Beleggia, M., Heller, L., & Šittner, P. (2009). Magnetostatic interactions and forces between cylindrical permanent magnets. *Journal of Magnetism and Magnetic Materials*, 321(22), 3758-3763.

Laidani, A., Bouhamida, M., Benghanem, M., Sammut, K., & Clement, B. (2019). *A Low-Cost Test Bench for Underwater Thruster Identification*. *IFAC-PapersOnLine*, 52(21), 254-259.

Lauder, B. E., & Spalding, D. B. (1972). *Lectures in Mathematical Models of Turbulence*. New York, Academic Press

## APPENDICES

### Appendix A: Test Calibrations

Besides the main testing, which was done as part of the experimental method to determine the feasibility of the thruster to generate force, several other tests were conducted with data collected to verify and validate the magnetic clutch's abilities.

#### Rotations Speed

Revolutions per minute, or RPM, measure how fast a rotating object turns. Knowing how fast an object turns is important in determining speed, gear ratios, how powerful a motor is, and how well the input shaft will transfer rotation to the output shaft. To calculate RPM, we used a tachometer and some reflective tape on the propeller and the input shaft.



*Figure A.1* Tachometer



*Figure A.2 Reflective Tape Set up*

The testing gave us the following data points

Table A.1: RPM Measurements

Volts	RPM
6	60
12	110
18	165
24	365

From this, we can verify the speed, and the gear ratio is confirmed to be 1:20.

### **Slip and Torque**

The following was a test done to find the force required to achieve "breakage". When the magnetic forces of the clutch could no longer overcome torque applied in the opposite direction, this was added as further work once it was discovered that a blockage on the output shaft would stop the input shaft completely and not still turn freely as previously predicted.

Through various iterations, the final version of the testing unit was constructed using 3D printed parts made from Pla+. It was constructed into three parts for ease of construction and included a solid steel rod for support. One side will hold the clutch, and the other side is designed to hold the rod up to keep the clutch level and horizontal. A hook was designed to attach to the input shaft, while the output shaft was designed to stay stationary and statically held in place. Notches are used to take measurements of the angle of deflection experienced from the provided force generated by the addition of weights hung by a hook to produce a point force.



*Figure A.3 Slip and Torque Test Set up*

*Table A.2 Slip and Torque Test Results*

Weight Applied	Deflection Angle
10	0
20	1
30	3
50	7
60	9
70	10
80	14
10	17
110	18
120	19
130	19
150	20
160	21
170	23
180	24
200	26
210	27
220	28
230	29
250	30
260	32
270	33
280	35
300	Snap

From the collected data, we can find the value to be between 280-300 g. Torque is calculated by  $T = D \cos\theta W$ , where  $D$  is the length of the hook used which is 4 inches.

Test restrictions we caused by the limited number of hanging weights available. We only had one of the following weights: 10g, 20g, 50g, 100g, and 200g. This caused the missing data points from the weights ending in 40g and 90g. For these data points, it would be acceptable to linear interpolate.

### **Balance Test**

The following was a test done to ensure the testing unit recorded the correct data without interference from the testing apparatus. An attachment was designed to add to the upper arm to load weights on a point. This was done for two reasons: (1) use the same distance apart to negate any differences in moment forces (2) to allow the weights to be applied to a point, so the force acts on one point.

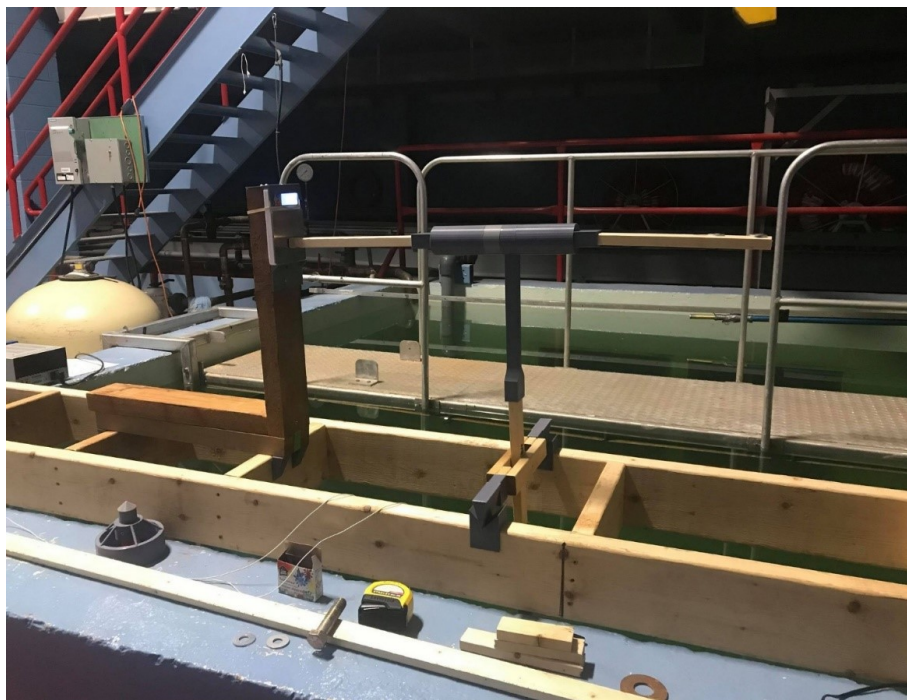


*Figure A.4 Balance Test Set Up*



Before the test started, each weight was checked on the scale to ensure the scale gave correct values. Then, the unit was set up, and the scale was zeroed each time before adding the weight. Enter values that were recorded from checking the scale horizontally and vertically are presented in the tables below.

Horizontal Results		
Grams Applied	Grams Recorded	% Error
500	501.33	-0.14
200	200.17	-0.04
100	99.62	0.19
50	49.31	0.70
20	20.01	0.025

*Table A.3* Horizontal Results

Vertical Results		
Grams Applied	Grams Recorded	% Error
500	415.21	9.27
200	174.04	6.94
100	87.73	6.55
50	48.03	2.01
20	22	4.76

*Table A.4* Vertical Results

From the results, we can calculate the range of error on this test to be around 2% due to the threshold the data is covered under. This number can be used for calibration of the testing unit.

## Magnet Point Load

We conducted a few tests on a point magnet model to find  $Q$  for our model set up. The photo below will show the setup used. For this, the gap was a set distance and weights were added until the parts separated. This could always be used as another way to predict our torque vs angle model data with the main drawback that is it measures the force for just one gap. Another issue was that our magnets are finite and not points. This is why we developed and conducted the testing using the slip and torque testing apparatus.

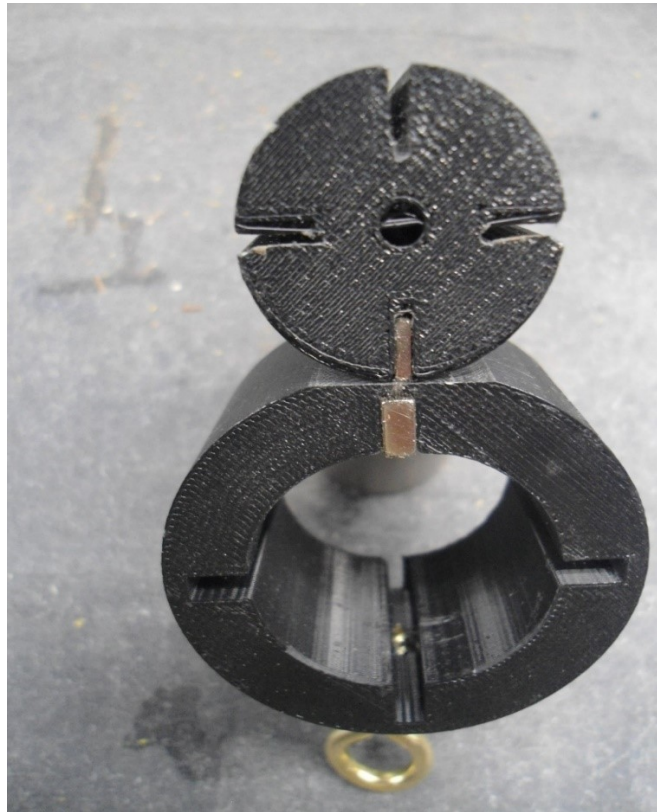
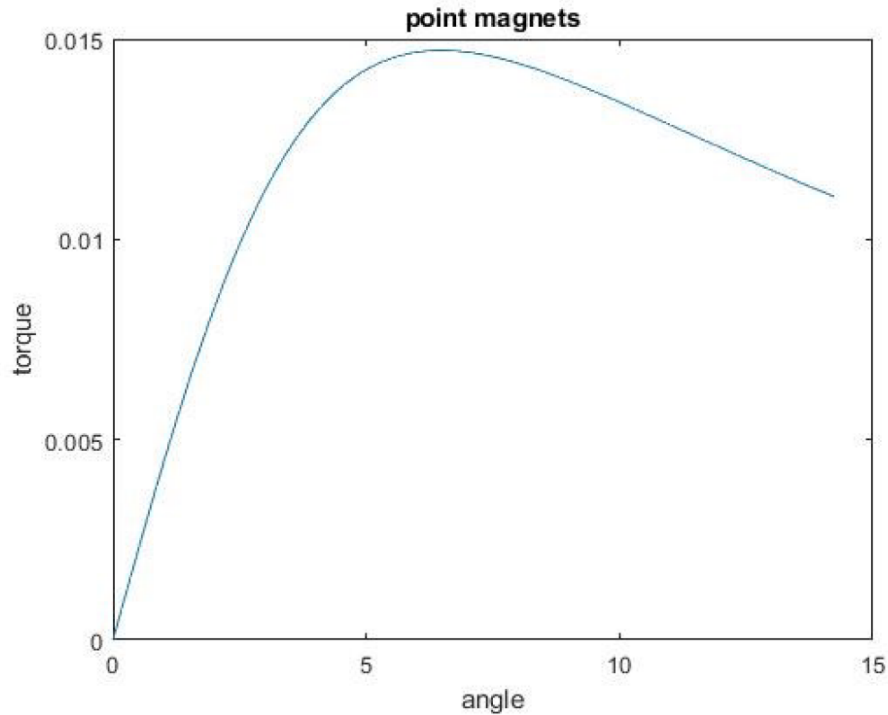


*Figure A.5 Magnet Point Load Test Set Up*

For a complete range, which could be studied in future work, one would have to conduct the test for different set points to determine the values needed. Then, an accurate prediction could be made using the magnetostatics model in ANSYS.

The data can be used to estimate the rotor torque using a point magnet model.



*Graph A.1: Magnet Load vs Angle*

### **Stream Flow Check**

One way we can use CFD is to display Streamlines. This is done by running a simulation to visually demonstrate the trajectories of the flow. These are the lines that are everywhere parallel to the velocity vectors at a fixed time. They consider only the direction of velocity, and not speed. It's a snapshot of flow at a moment in time. To compare the flow stream from that which we have seen from CFD, Drops of food coloring was put in front of the thruster while it was in operation. With this we were able to record and visually see a pattern like that of simulation streamlines. If you plot them and turn on the glyphs, you will see that they are similar. In other words, if the flow field is steady-state and you would put a

particle on the start of one path-line (trajectory), the particle will flow through the domain as indicated by the streamline/trajectory.

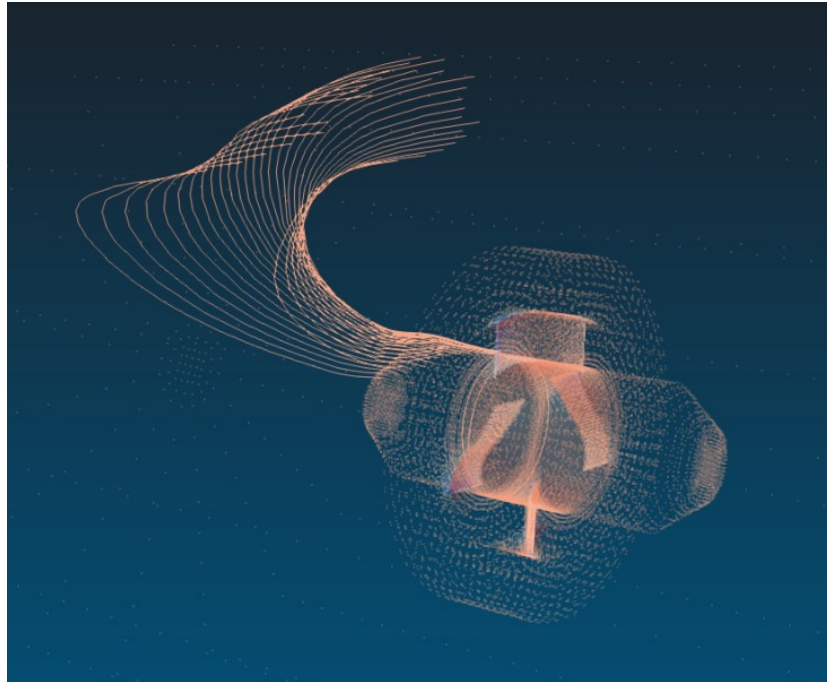


*Figure A.6* CFD Streamline

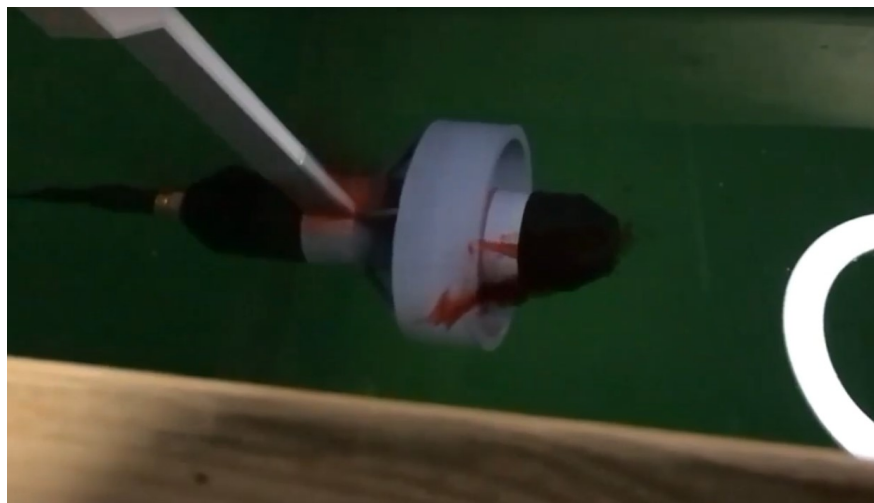


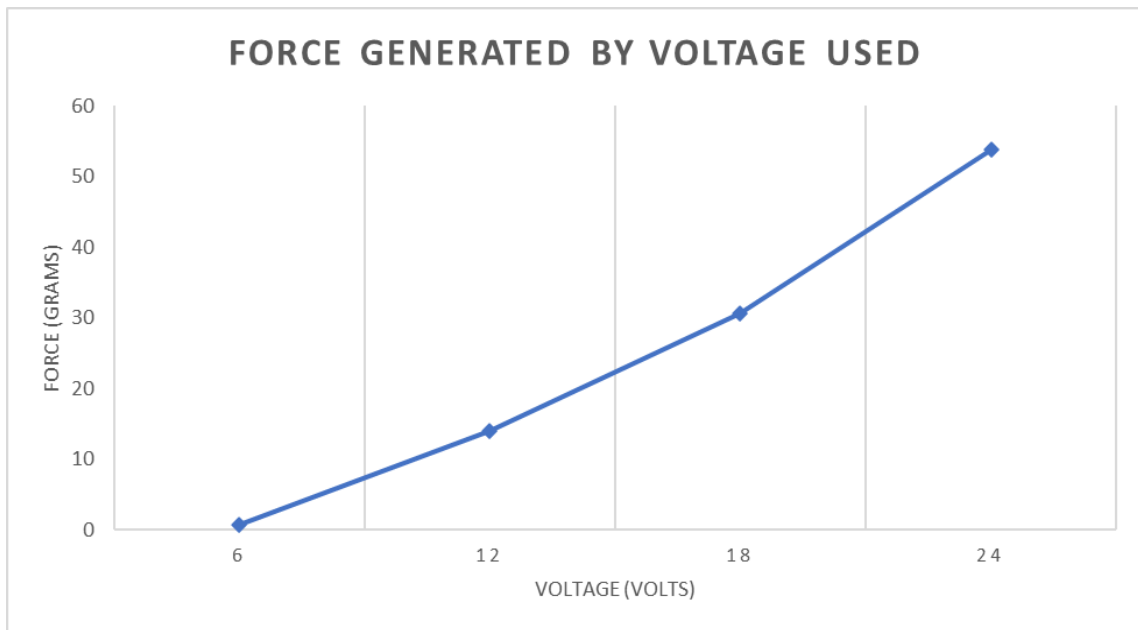
*Figure A.7* Red Dye Test

## Appendix B: Raw Test Data

### Test 1

The first test has the thruster partially submerged in water with one inch of the prop left out. The following data was collected

Voltage (V)	Current (Amp)	Force (Grams)
6	0.02	0.71
12	0.035	14.02
18	0.05	30.66
24	0.07	53.8

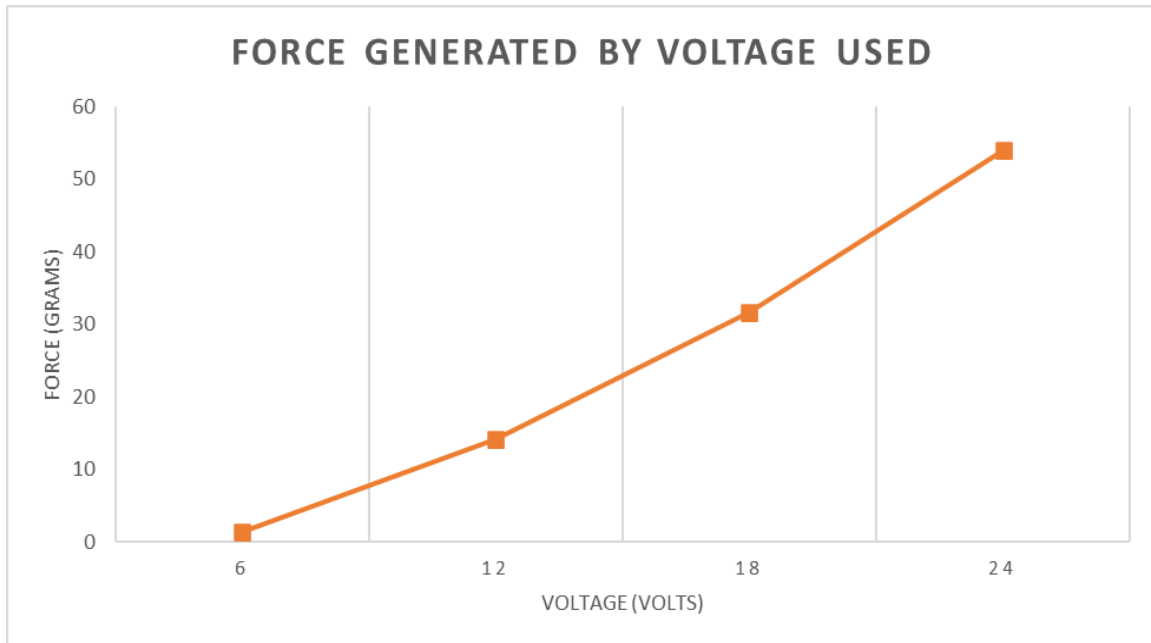


*Graph B.1* Test 1 Results

## Test 2

The second test has the thruster fully submerged in water with one inch of water above the prop. The following data was collected

Voltage (V)	Current (Amp)	Force (Grams)
6	0.02	1.45
12	0.035	14.22
18	0.05	31.60
24	0.07	54.00

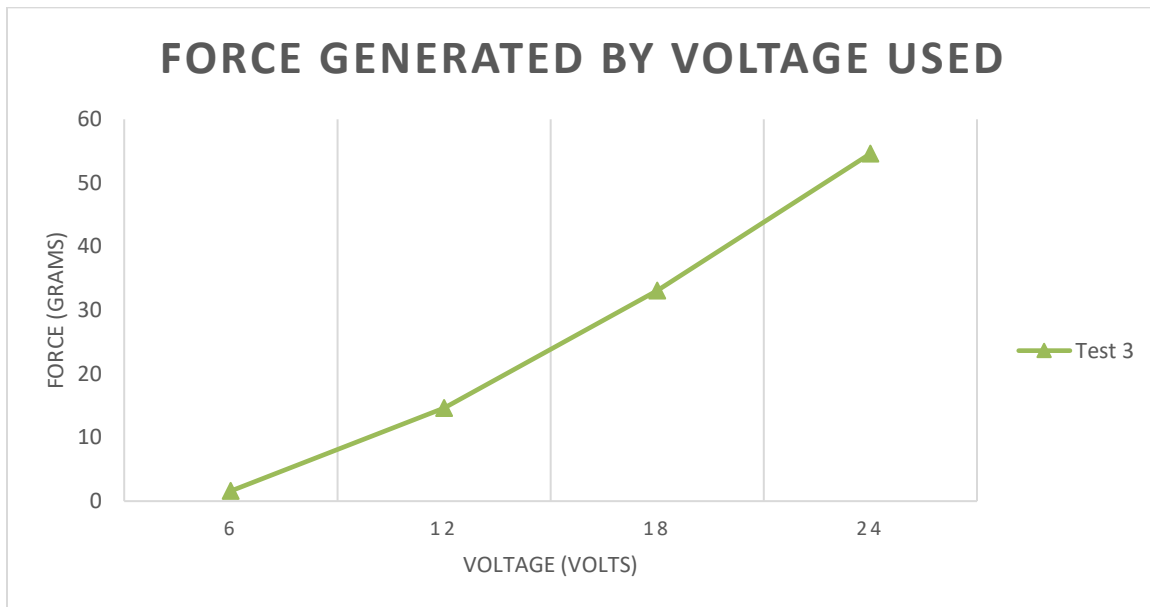


*Graph B.2 Test 2 Results*

### Test 3

The third test has the thruster fully submerged in water with one full prop diameter (100mm or 4 inches) of water above the prop. The following data was collected.

Voltage (V)	Current (Amp)	Force (Grams)
6	0.02	1.60
12	0.035	14.61
18	0.05	33.08
24	0.07	54.60

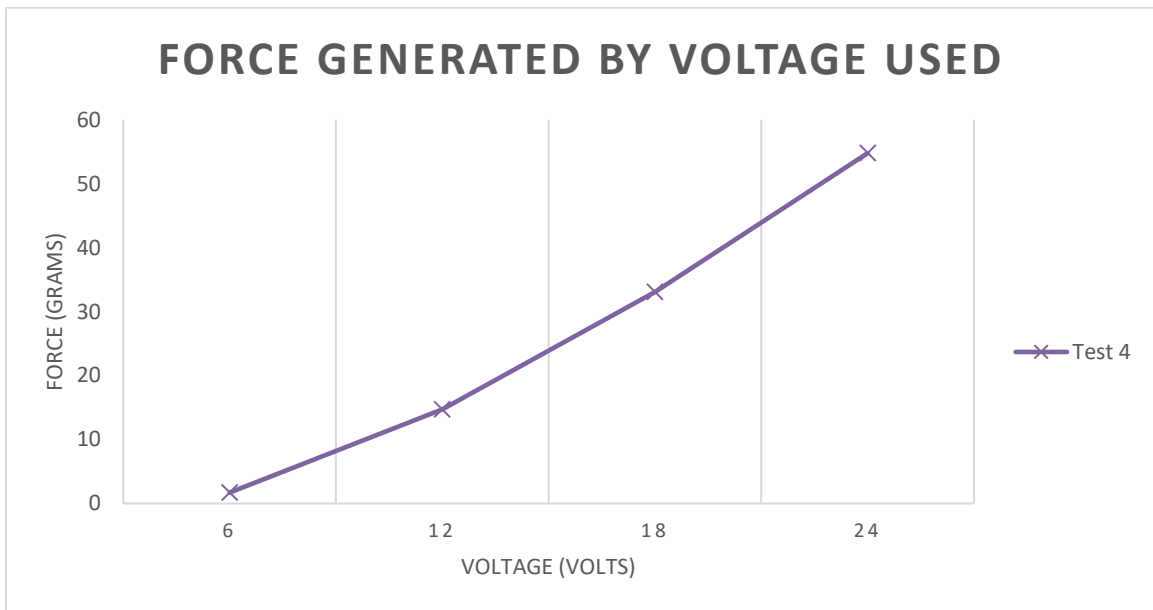


*Graph B.3 Test 3 Results*

### Test 4

The Fourth test has the thruster fully submerged in water with two full prop diameters (200mm or 8 inches) of water above the prop. The following data was collected

Voltage (V)	Current (Amp)	Force (Grams)
6	0.02	1
12	0.035	14.7
18	0.05	33.05
24	0.07	54.76



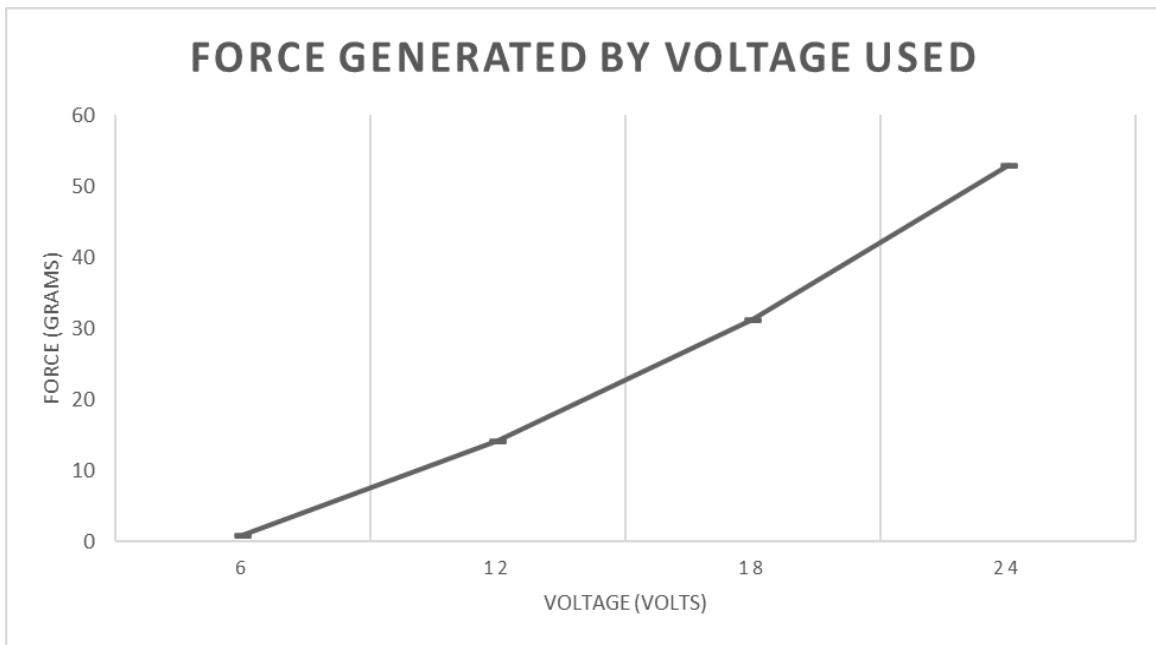
*Graph B.4 Test 4 Results*



### Test 5

The fifth test has the thruster fully submerged in water with two full prop diameters (200mm or 8 inches) of water above the prop. The difference between test 4 is that the direction of rotation of the propeller has been reversed. The following data was collected

Voltage (V)	Current (Amp)	Force (Grams)
6	0.02	1
12	0.035	14.2
18	0.05	31.3
24	0.07	53

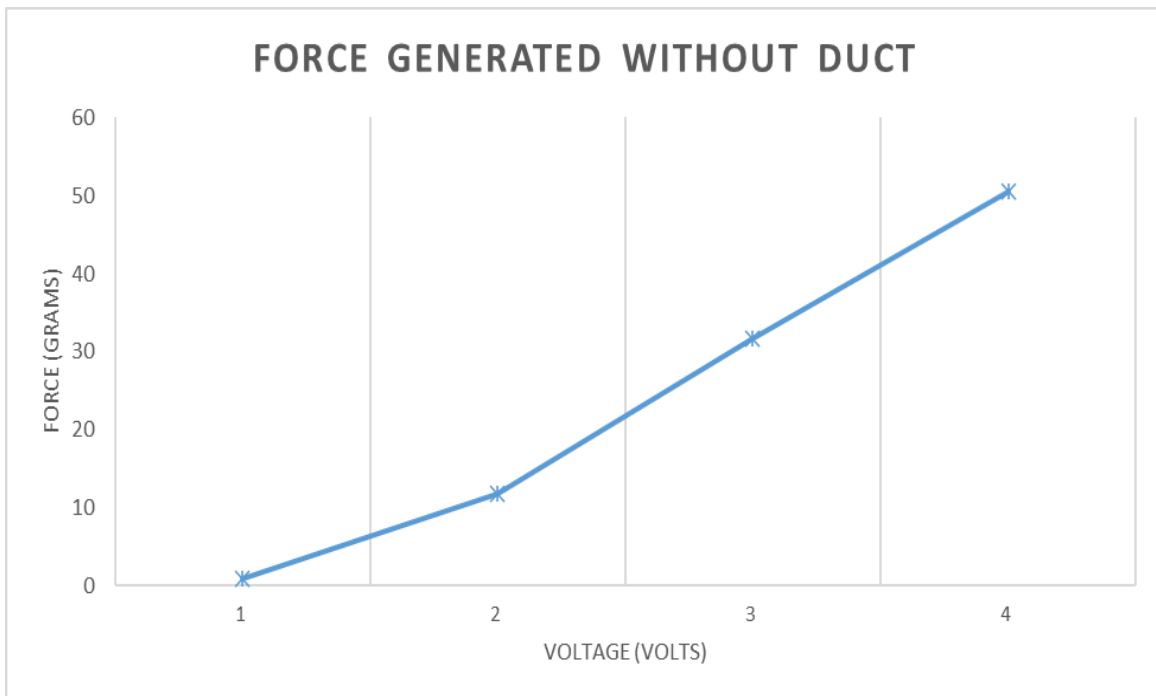


*Graph B.5 Test 5 Results*

## Test 6

The sixth test has the thruster fully submerged in water with two full prop diameters (200mm or 8 inches) of water above the prop. The difference between test 4 is that the Duct has been removed. The following data was collected

Voltage (V)	Current (Amp)	Force (Grams)
6	0.02	1
12	0.035	11.83
18	0.05	31.73
24	0.07	50.51

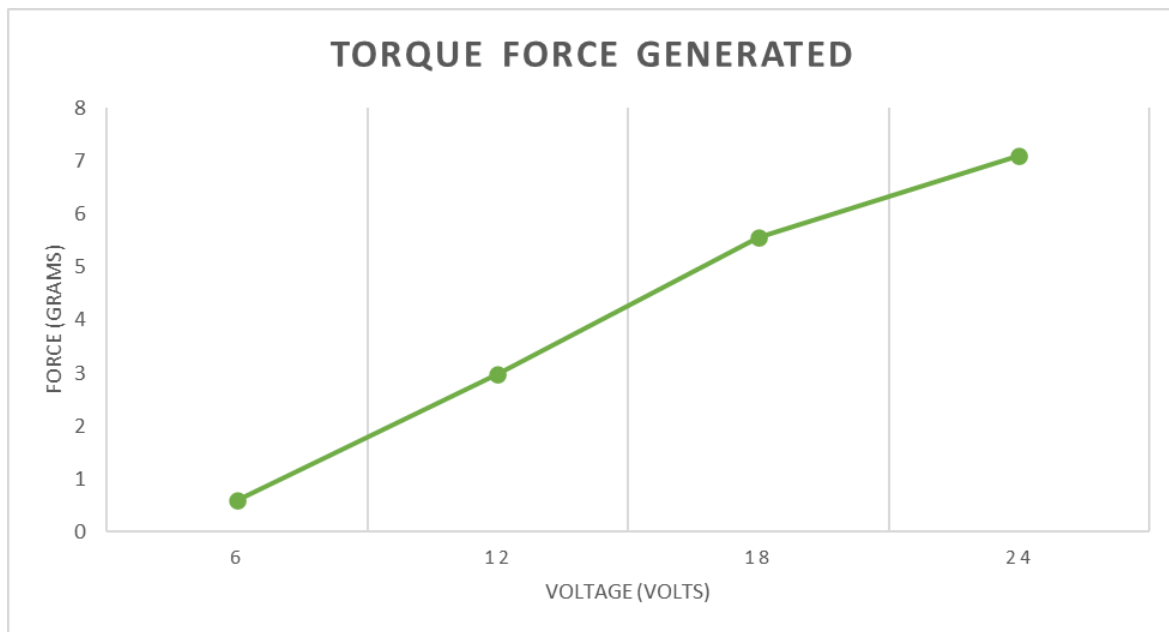


*Graph B.6 Test 6 Results*

## Test 7

The seventh test has the thruster fully submerged in water with two full prop length (200mm or 8 inches) of water above the prop. The prop has been turned 90 degrees, with the front endcap facing the closest wall of the deep tank. It is hooked up to the attachments used to allow the testing rig to test the force generated by torque. The following data was collected

Voltage (V)	Current (Amp)	Force (Grams)
6	0.02	0.6
12	0.035	2.97
18	0.05	5.55
24	0.07	7.1

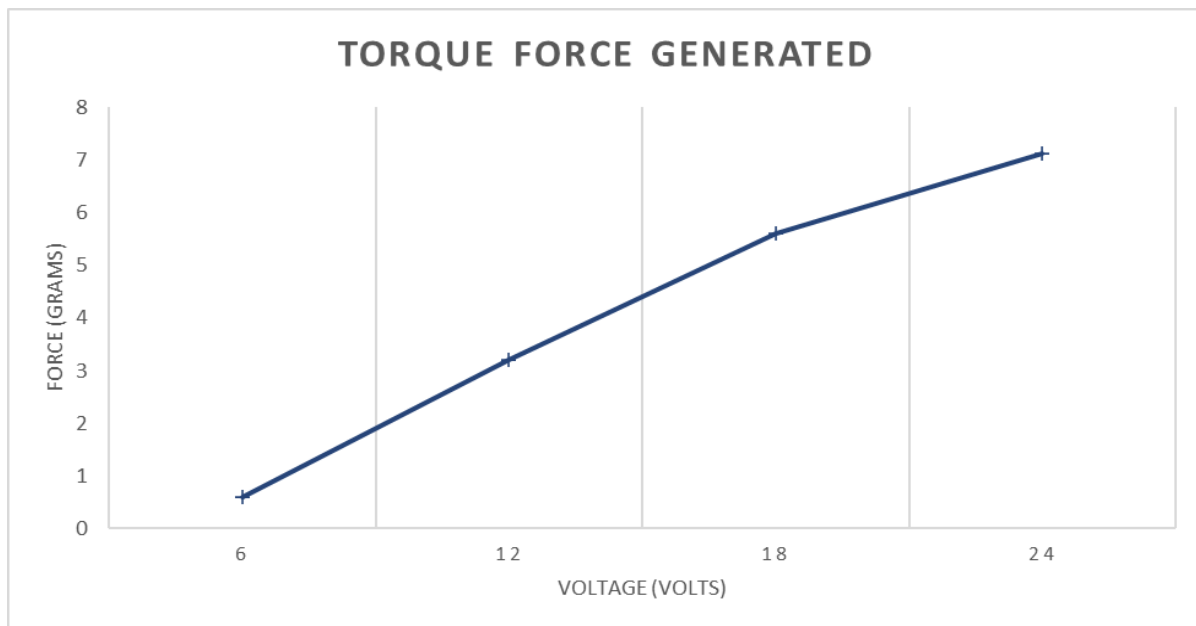


*Graph B.7 Test 7 Results*

## Test 8

The eighth test has the thruster fully submerged in water with two full prop diameters (200mm or 8 inches) of water above the prop. The prop has been turned 90 degrees, with the front endcap facing the closest wall of the tank. It's hooked up to the attachments to allow the testing right to test the force generated by torque. The testing unit is moved out to the middle of the deep tank. The following data was collected.

Voltage (V)	Current (Amp)	Force (Grams)
6	0.02	0.6
12	0.035	2.97
18	0.05	5.55
24	0.07	7.1

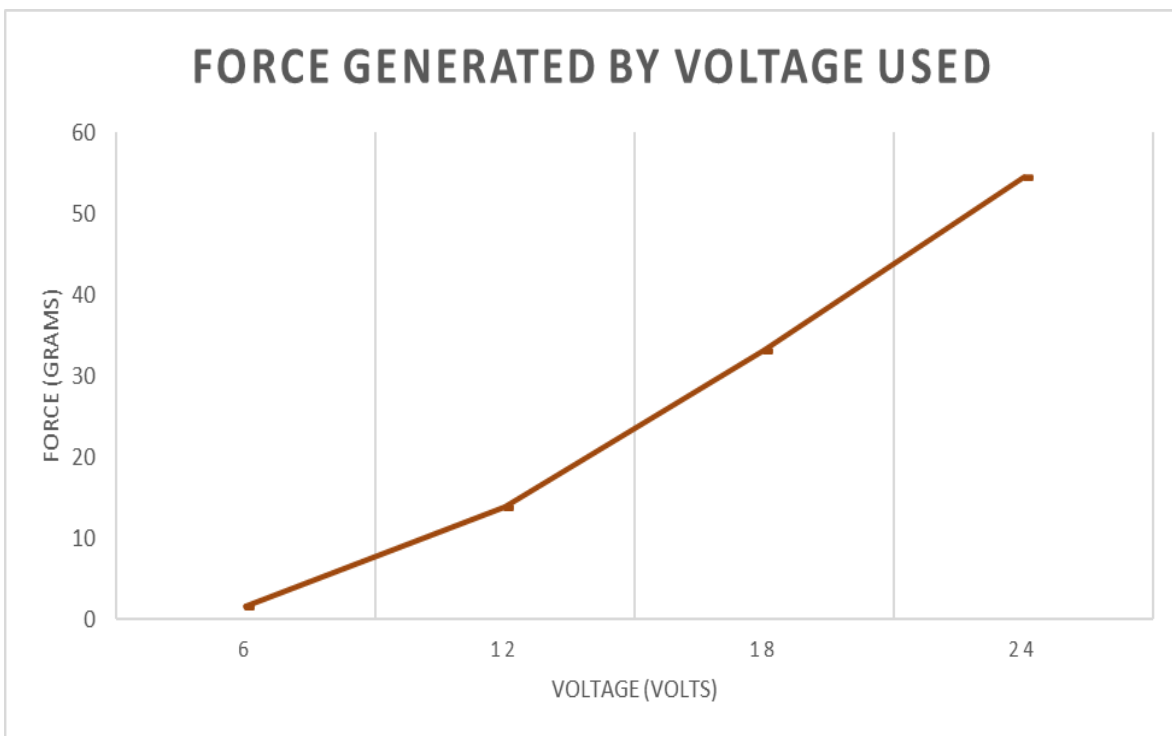


*Graph B.8 Test 8 Results*

## Test 9

The ninth test has the thruster fully submerged in water with two full prop diameters (200mm or 8 inches) of water above the prop. The testing unit is moved out to the middle of the deep tank. The following data was collected.

Voltage (V)	Current (Amp)	Force (Grams)
6	0.02	1.6
12	0.035	13.8
18	0.05	33.1
24	0.07	54.6



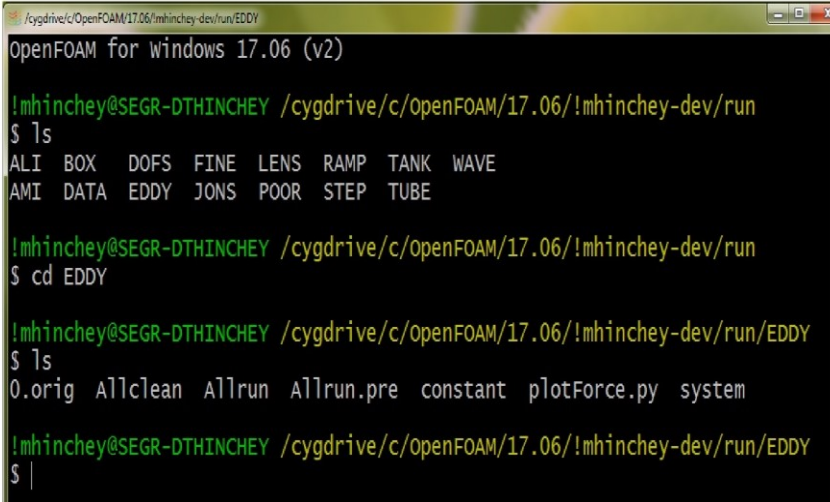
*Graph B.9* Test 9 Results

## Appendix C: Openfoam Menus

OpenFoam is an open-source computational fluid dynamics software. Users can modify any of its codes. It has numerous tutorials that have been generated mainly by users. The current work is based on a tutorial called “propeller”.

OpenFoam can handle many different flows. The current work uses the solver for an incompressible and viscous fluid. The governing equations are conservation of mass and conservation of momentum. In addition, the  $k\epsilon$  eddy viscosity model is used to approximate the influence of turbulence.

Setting up an OpenFoam simulation is done by modifying text files in a folder in the C drive of a host computer. Then, it is run through an icon on the desktop of the computer. The run window is given in Figure C.1 below:



```
OpenFOAM for windows 17.06 (v2)
!mhinchey@SEGR-DTHINCHEY /cygdrive/c/OpenFOAM/17.06/!mhinchey-dev/run
$ ls
ALI BOX DOFS FINE LENS RAMP TANK WAVE
AMI DATA EDDY JONS POOR STEP TUBE

!mhinchey@SEGR-DTHINCHEY /cygdrive/c/OpenFOAM/17.06/!mhinchey-dev/run
$ cd EDDY

!mhinchey@SEGR-DTHINCHEY /cygdrive/c/OpenFOAM/17.06/!mhinchey-dev/run/EDDY
$ ls
0.orig Allclean Allrun Allrun.pre constant plotForce.py system

!mhinchey@SEGR-DTHINCHEY /cygdrive/c/OpenFOAM/17.06/!mhinchey-dev/run/EDDY
$ |
```

*Figure C.1* Run Window

The thesis case is EDDY. The contents of EDDY are:

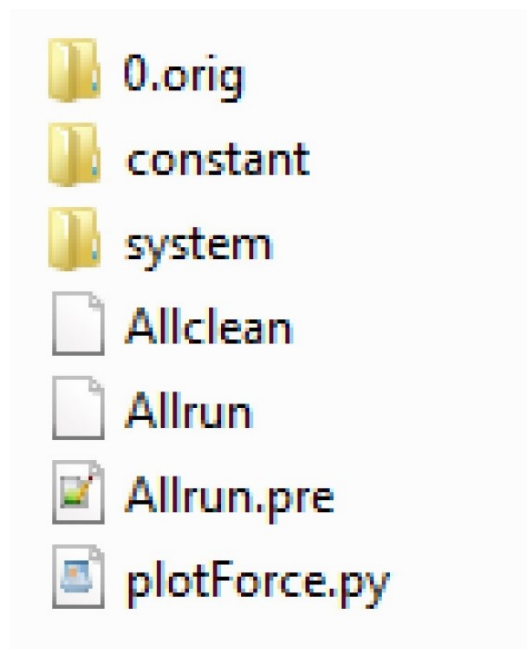


*Figure C.2 Eddy Folder Contents*

The run function [Allclean] removes files generated in the last run. The run function [Allrun.pre] creates the files needed to run a simulation. The run function [Allrun] runs the simulation.

The contents of the 0.orig folder are:

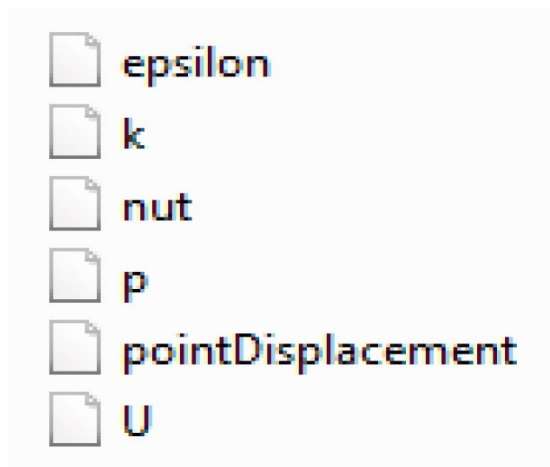


*Figure C.3 0.orig Folder Contents*

These text files give the solution variables on the boundary of the solution domain and within it at the beginning of the simulation.

The contents of the constant folder are:

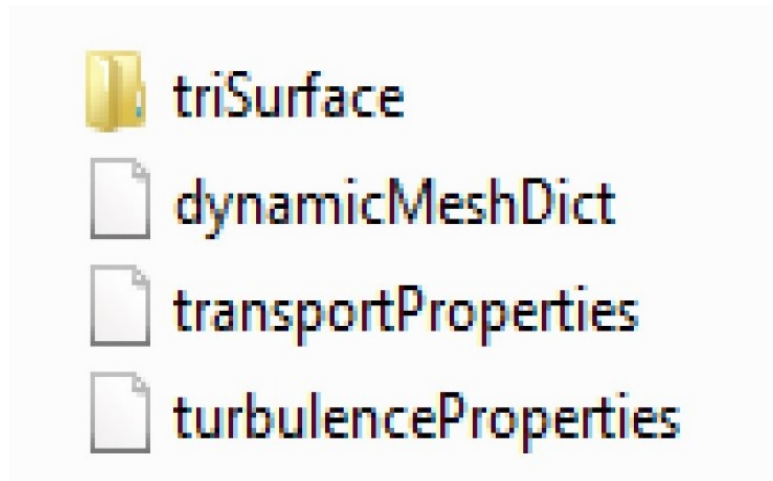


*Figure C.4* Constant Folder Contents

By default, OpenFOAM defines a mesh of arbitrary polyhedral cells in 3-D, bounded by arbitrary polygonal faces, i.e., the cells can have an unlimited number of faces where, for each face, there is no limit on the number of edges nor any restriction on its alignment. A mesh with this general structure is known as a polyMesh. We kept this type of mesh because it offers great freedom in mesh generation and manipulation, in particular when the geometry of the domain is complex or changes over time.

The [dynamicMeshDict] file sets the steady state speed of the propeller. It assumes that the flow reaches a steady state. The kinematic viscosity of water is given in the [transportProperties] file. The density of the working fluid is assumed to be unity. Unity results are multiplied by 1000 to get results for water. The turbulence model is set in the [turbulenceProperties] file.



The contents of the triSurface subfolder are:

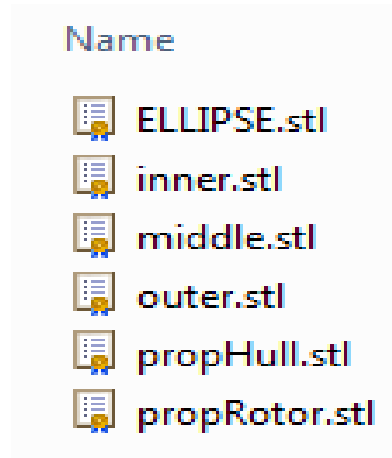


*Figure C.5* TriSurface Subfolder Contents

The geometry of the propeller is contained in the STL files [propHull.stl] and [propRotor.stl]. these were created from out CAD model and then formatting it into the stereolithography STL file needed. This can be done by modifying the parts from the 3d printing portion of the project and saving them as an STL as a complete model.

The solution domain is divided into a part that spins and a part that does not spin. The part that spins is contained in the STL file [inner.stl]. The rotor of the propeller is inside the inner. The part of the domain that does not spin is divided into two parts given by [middle.stl] and [outer.stl]. The middle part is a buffer between the outer and inner parts.

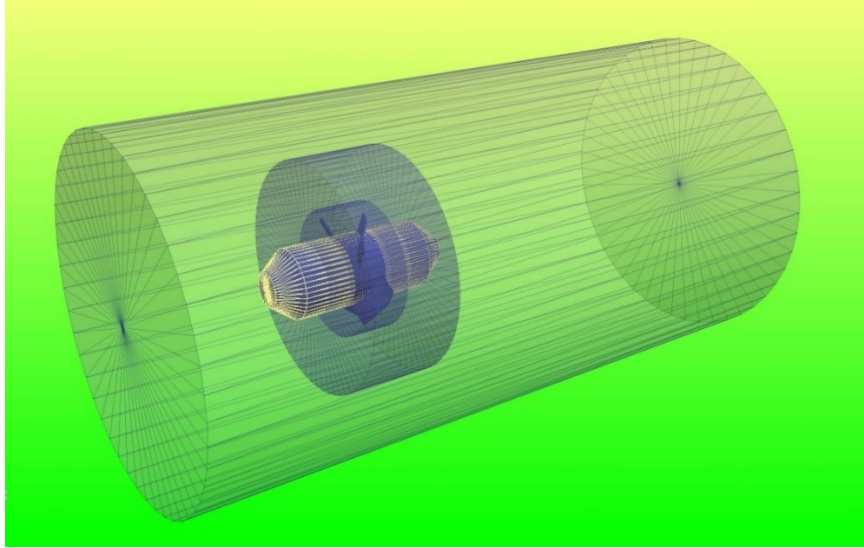


*Figure C.6 Dynamic Meshes*

The contents of the system folder are:

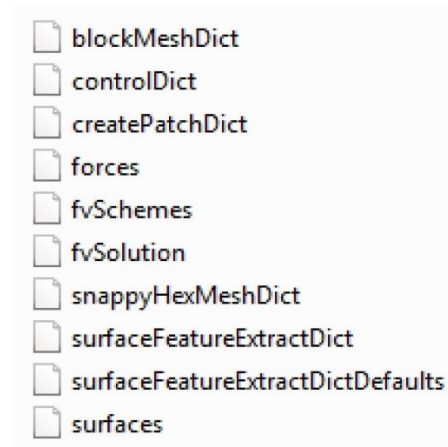


*Figure C.7 System Folder Contents*

These files focus on the creation of a grid or mesh. The most important files are [blockMeshDict], [snappyHexMeshDict] and [surfaceFeatureExtractDict].

Since our shape is considered complex, we used snappyHexMesh, a mesh generator chisel. But for this, it requires:

1. A very well-defined dictionary, namely system/snappyHexMeshDict.
2. Good geometrical definitions, such as STL/OBJ files with well-defined surfaces;
3. eMesh feature edge files that define feature edges that have to describe sharp corners.

The mesh needs to be defined the most at the complex features where we wanted to see the most important data. The project used the finer mesh at the propeller and simpler on the body of the thruster. This helped with computing time.

## Appendix D: Hydrodynamic Bearing

Lubrication flows are low Reynolds Number flows. They are governed by Reynolds Equation for Pressure. The derivation of this is beyond the scope of this thesis.

For a cylindrical geometry, Reynolds Equation is

$$\begin{aligned} \frac{\partial}{\partial r} \left( \frac{rh^3}{12\mu} \frac{\partial P}{\partial r} \right) + r \frac{\partial}{\partial c} \left( \frac{h^3}{12\mu} \frac{\partial P}{\partial c} \right) \\ = \frac{\partial}{\partial r} \left( \frac{rh(U_\tau + U_B)}{2} \right) + \frac{\partial}{\partial \Theta} \left( \frac{h(V_\tau + V_B)}{2} \right) + r(W_\tau + W_B) \end{aligned}$$

*Equation D.1* Reynolds Equation

where P is pressure, U is radial velocity, V is circumferential velocity, W is normal velocity, r is the radial coordinate, c and  $\Theta$  are the circumferential distance and angular coordinates respectively, h is gap and  $\mu$  is viscosity.

Manipulation gives

$$r \frac{\partial}{\partial c} \left( h^3 \frac{\partial P}{\partial c} \right) + \frac{\partial}{\partial r} \left( rh^3 \frac{\partial P}{\partial r} \right) = 6\mu S \frac{\partial h}{\partial \Theta}$$

*Equation D.2* Thrust Bearing Case

where S is the bearing tangential speed. This is radius times rotational speed.

Analytical solutions are generally not possible for 2D geometries. Solutions can only be obtained using CFD. Analytical solutions are possible for certain 1D geometries. An example is a bearing with blocked sides. For the propeller bearing, this would be its outer and inner edges. The inner edge is naturally blocked. The outer edge could be blocked with a wiper.

For a bearing with blocked sides, Reynolds Equation becomes

$$\frac{\partial}{\partial c} \left( h^3 \frac{\partial P}{\partial c} \right) = 6\mu S \frac{\partial h}{\partial c}$$

*Equation D.3 Blocked Sides Case*

The propeller used a step bearing. For this, there is a jump in gap from one constant level to another constant level. The pressure gradient equation shows that the gradient is constant in the constant gap regions. This means that the pressure variation is linear in the constant gap regions.

Let the peak pressure be **P**. Let the front gap be **b** and let the back gap be **a**. Let the length of the front region be **w** and the length of the back region be **v**. Across the step, one can write

$$\Delta \left( h^3 \frac{\Delta P}{\Delta c} \right) = H \Delta h$$

*Equation D.4 Step Bearing Case*

where H is  $6\mu S$ . Substitution into this gives

$$a^3 \frac{(0 - P)}{v} - b^3 \frac{(P - 0)}{w} = H(a - b)$$

*Equation D.5 Simplified Step Case*

Manipulation gives

$$P = H \frac{(b - a)}{\left( \frac{a^3}{v} + \frac{b^3}{w} \right)}$$

*Equation D.6 Step Pressure*

This equation shows that, as the gaps **a** and **b** are made very small, the pressure **P** and thus the thrust **T** both tend to infinity. At very low gaps, viscous shear would counteract this. The torque required to spin the propeller would increase dramatically.

## Appendix E: Simple Propeller Model

A propeller gathers water from far upstream and throws it downstream as a jet. Conservation of momentum for a control volume surrounding the water gives

$$R = \rho Q U$$

*Equation E.1 Jet Thrust Equation*

where  $R$  is the reaction or thrust force on the propeller,  $U$  is the speed of the jet,  $\rho$  is the density of water and  $Q$  is the volumetric flow through the propeller. The speed of the jet depends on the rotation speed of the propeller. Geometry gives

$$\tan[\beta] = \frac{U}{V}$$

*Equation E.2 Flow Geometry*

where  $\beta$  is the propeller blade angle at the rear and  $V$  is the blade trailing edge speed due to rotation. This gives

$$U = V \tan[\beta]$$

*Equation E.3 Jet Speed Equation*

The speed due to rotation  $V$  is  $r\omega$  where  $r$  is the average radius out to the blade and  $\omega$  is the rotational speed of the blade. The volumetric flow rate  $Q$  is  $U A$  and flow area  $A$  is  $2\pi r \Delta r$ .

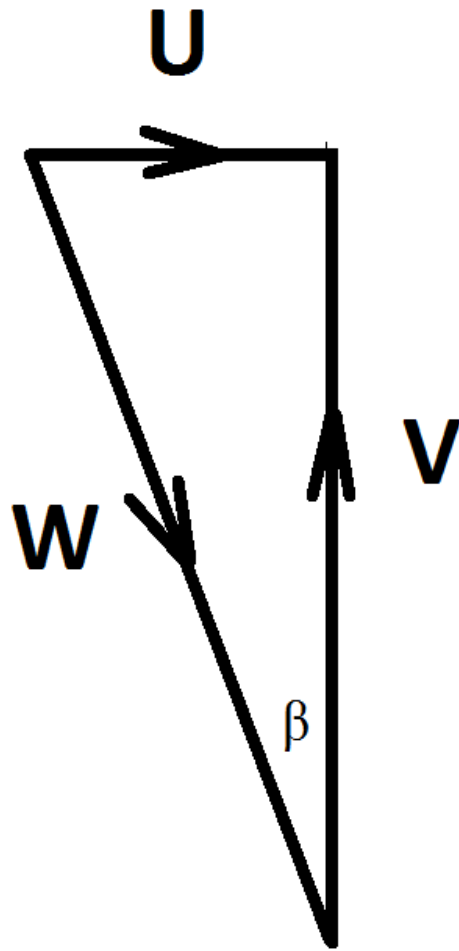


Figure E.1 Velocity Vector Diagram

### Sample Thrust Calculation

The rotational speed of the propeller is 300 RPM or 5 RPS or

$$\omega = 2\pi \cdot 5 = 31.4 \text{ r/s}$$

The propeller geometry gives

$$r = 0.04\text{m} \quad \Delta r = 0.02\text{m}$$



The blade angle  $\beta$  at the rear is 15 degrees. The density of water is  $1000 \text{ kg/m}^3$ .

$$V = r\omega = 0.04 * 31.4 = 1.26 \text{ m/s}$$

$$U = V \tan[\beta] = 1.26 * \tan[15] = 1.26 * 0.27 = 0.34 \text{ m/s}$$

$$A = 2\pi r \Delta r = 2\pi * 0.04 * 0.02 = 0.005 \text{ m}^2$$

$$Q = U A = 0.34 * 0.005 = 0.0017 \text{ m}^3/\text{s}$$

$$R = \rho Q U = 1000 * 0.0017 * 0.34 = 0.58 \text{ N}$$

$$0.58 \text{ N} = 0.059 \text{ kg} = 59 \text{ g}$$

## Appendix F: Hull Hoop Stress

The hull tube would be subjected to external hydrostatic pressure. This would put its wall under compressive hoop stress. The hoop stress is

$$\sigma = \frac{p r}{t}$$

*Equation F.1 Hoop Stress*

where  $\sigma$  is the hoop stress,  $p$  is the external pressure,  $r$  is the radius of the tube and  $t$  is its wall thickness.

Manipulation gives the pressure equation

$$p = \frac{\sigma t}{r}$$

*Equation F.2 External Pressure*

The maximum compressive stress of stainless steel is about 250 MPa. The radius is 0.5” or 0.0127 m and the thickness is 0.0625” or 0.0016 m

$$p = 250000000 * \frac{0.0016}{0.0127} = 31.5 \text{ MPa}$$

The pressure depth law gives

$$p = \rho g h$$

*Equation F.3 Pressure Depth Law*

Manipulation gives

$$h = \frac{p}{\rho g}$$

*Equation F.4* Operation Depth

$$= 31500000 / 1000 / 9.81 = 3211 \text{ m}$$

Our AUV maximum depth is around 100 m. So we have a factor of safety of 32.